Comprehensive Study of Sodium, Copper, and Silver Clusters Over a Wide Range of sizes 2 N 75

doi: 10.1063/1.3187934

Comprehensive study of sodium, copper, and silver clusters over a wide range of sizes $2 \leq N \leq 75$

Masahiro Itoh,[1,2,a)] Vijay Kumar,[1,3] Tadafumi Adschiri,[2] and Yoshiyuki Kawazoe[1]
[1]*Institute for Materials Research, Tohoku University, Aoba-ku, Sendai 980-8577, Japan*
[2]*Institute of Multidisciplinary Research for Advanced Materials, Tohoku University, Aoba-ku, Sendai 980-8577, Japan*
[3]*Dr. Vijay Kumar Foundation, 45 Bazaar Street, K. K. Nagar (West), Chennai 600 078, India*

(Received 3 February 2009; accepted 29 June 2009; published online 6 November 2009; publisher error corrected 10 November 2009)

The geometric and electronic structures of Na_N, Cu_N, and Ag_N metal clusters are systematically studied based on the density functional theory over a wide range of cluster sizes $2 \leq N \leq 75$. A remarkable similarity is observed between the optimized geometric structures of alkali and noble metal clusters over all of the calculated cluster sizes N. The most stable structures are the same for the three different metal clusters for approximately half the cluster sizes N considered in this study. Even if the most stable structures are different, the same types of structures are obtained when the metastable structures are also considered. For all of the three different metal clusters, the cluster shapes change in the order of linear, planar, opened, and closed structures with increasing N. This structural-type transition leads to a deviation from the monotonic increase in the specific volume with N. A remarkable similarity is also observed for the N dependence of the cluster energy $E(N)$ for the most stable geometric structures. The amplitude of this energy difference is larger in the two noble metal clusters than in the alkali metal cluster. This is attributed to the contribution of d electrons to the bonds. The magic number is explicitly defined with a new criterion in the framework of total energy calculations. In the case of Na_N, a semiquantitative comparison between the experimental abundance spectra [Knight *et al.*, Phys. Rev. Lett. **52**, 2141 (1984)] and the total energy calculations is carried out. The changing aspect of the Kohn–Sham eigenvalues from $N=2$ to $N=75$ is presented for the three different metal clusters. The feature of the bulk density of states already appears at $N=75$ for all of three clusters. With increasing N, the highest occupied molecular orbital (HOMO)-lowest unoccupied molecular orbital (LUMO) gap clearly exhibits an odd-even alternation and converges to 0. Although there is a similarity in the N dependence of the HOMO-LUMO gap between the three metal clusters, it is much stronger between the two noble metal clusters. The growth aspect of the d band below the Fermi level of the noble metal clusters with increasing N is presented. A good correspondence is observed in the d characteristic of the electronic states between the cluster composed of 75 atoms and the bulk metal. The similarities observed in the N dependence of the geometric structures and $E(N)$s originate from the similarity in that of the electronic structures. © *2009 American Institute of Physics*. [doi:10.1063/1.3187934]

I. INTRODUCTION

It is beneficial to study the geometric structures and various electronic properties of clusters as an intermediate phase of materials between isolated and condensed systems; the combination of quantum chemistry and solid state physics will result in further developments in the field of materials science. In the basis of the density functional theory (DFT),[1,2] an *ab initio* many-body theory for systems in the ground state, a detailed comparative study of the most and metastable geometric and electronic structures of three different metal clusters—Na_N, Cu_N, and Ag_N—is systematically carried out over a wide range of $2 \leq N \leq 75$. The three types of atoms composing those clusters have a common feature in that the outermost valence electron is one s electron. The changing and converging aspects of the geometric and electronic structures of alkali and noble metal clusters from a diatomic molecule (dimer) to a condensed system have been presented explicitly and compared for the first time. A simple review of previous studies on clusters is presented below.

In 1984, a study was carried out based on the Woods–Saxon-type shell model[3] to explain the distinctive peak observed in the abundance spectra of a Na_N cluster at special value of N ($N=8,20,40,58,92,\ldots$) evaluated in an experiment. Within this shell model, the electronic structures of simple metal clusters are expressed based on a simple spherical effective potential using phenomenological parameters. In this model, the Coulomb interactions between electrons are completely neglected. In a later study, Clemenger[4] explained the anomalous N-dependent stability of a Na_N cluster using a harmonic oscillator-type shell model with the effect of Coulomb interactions being neglected. In addition to simple shell models, various types of jellium models[5–8] were adopted for Na_N clusters. In jellium models for metal clus-

a)Electronic mail: itoh.japan@gmail.com.

ters, the equilibrium ionic configuration of a cluster is averaged and replaced by a uniform or nearly uniform potential with a surface boundary. In most previous studies, the jellium models were incorporated with the DFT and the total energies were evaluated. The subsequent calculations have shown that the simple models give correct shapes for neutral and charged Na_N clusters within a range of cluster sizes $2 \leq N \leq 21$.[9,10] Also the calculations are successful in giving correct energetics for charged Na_N clusters.[9] In model-based studies of Na_N, the N-dependent cluster stability was evaluated based on the shell correction energy, curvature of the sum of the electronic eigenvalues, and total energy.[6–8,11–19]

For the evaluation of the N-dependent total energy, a semiquantitative comparison with the peak intensity $I(N)$ in the experimental abundance spectra[20] was also carried out. However, cluster studies based on these models are different from those based on the first principles (FP) calculations, which directly relate the geometric structures to the electronic structures. Even if the experimental magic number for a particular value of N is obtained accidentally, these models are not based on a close relationship between the geometric and electronic structures of real Na_N clusters. Furthermore, using these models, it is impossible to study the similarities and differences between the alkali metal cluster Na_N and the noble metal clusters Cu_N and Ag_N because the s electron in the outermost shell as well as d electrons in the inner shell contribute to bonding in the latter.

Recently, the most and metastable structures of charge neutral Na_N, Cu_N, and Ag_N clusters were determined for $N \leq 22$ from FP calculations based on DFT.[21–27] In this study, an extremely systematic comparative study based on DFT was carried out for the three different metal clusters up to $N=75$. Our study successfully reproduced the results of stable geometric structures obtained in previous studies; furthermore, it successfully discovered the convergence aspects of the electronic structures of clusters with those of bulk metals.

In Sec. II, the computational method and the approximation are described. In Sec. III, the most and metastable structures are systematically classified and the similarities and differences between the three different metal clusters are described. In Sec. IV, the N dependence of the ground state energy of the most stable cluster structure is analyzed. In Sec. V, all aspects of the electronic structure of the clusters including the odd-even alternation of the highest occupied molecular orbital (HOMO)-lowest unoccupied molecular orbital (LUMO) gap are described. In Sec. VI, the conclusion of this study is presented.

II. COMPUTATIONAL METHODS

An exact many-body theory for a ground state system DFT (Refs. 1 and 2) was employed to study the geometric and electronic structures of Na_N, Cu_N, and Ag_N clusters. In the DFT, various physical properties of materials such as the exact ground state total energy can be evaluated if the exact exchange-correlation energy functional is adopted.

In this study, the generalized gradient approximation (GGA) proposed by Perdew and Wang[28] (PW91) is employed for the exchange-correlation energy functional. In this approximation, several physical properties such as interatomic distance and cohesive energy are well described in many systems. The spin polarization of the system was also considered.

In order to reduce the number of plane waves used in the calculation of the electronic structure, a pseudopotential method is employed for an approximation of the nucleus, inner core electrons, and valence electrons. An unempirical pseudopotential called ultrasoft pseudopotential[29] was employed. In a manner similar to other methods, relativistic correction terms such as the mass velocity and the Darwin terms are included in the pseudopotentials. For Na, Cu, and Ag atoms, $3s^1$, $3d^{10}4s^1$, and $4d^{10}5s^1$ electrons were explicitly treated as the valence electrons, respectively.

Instead of treating the isolated system as is, the total energy can be effectively converged by using a plane wave basis set within a reciprocal space representation, which is frequently used in periodic systems. Here, isolated systems are approximated by pseudocrystal systems constructed using arranged isolated systems having sufficient space between them.

In this method, the total energy can be effectively converged by simply increasing the cutoff energy of a plane wave expansion. The total energy of the cluster is approximately evaluated from the total energy of the pseudocrystal system per unit cell. Another advantage of employing this method is that it is possible to evaluate the total energies and electronic structures of the clusters and bulk solids using a single method.

The edge length of each cubic unit cell of the pseudocrystal systems was set to be 20–30 Å for Na_N clusters and 15–30 Å for Cu_N and Ag_N clusters. It was confirmed that these lengths are sufficiently large to neglect the electronic wave vector dependence in these electronic structures. The cutoff energies for the plane wave expansion were set to be 48.7, 233.7, and 180.7 eV for Na_N, Cu_N, and Ag_N, respectively. Brillouin zone integration was carried out only for the Γ-point in the pseudocrystal system. The residual minimization scheme, direct inversion in the iterative subspace algorithm was adopted for the effective self-consistent calculation of the electronic structures.[30,31] The convergence criterion of the total energy was set to be within 1×10^{-4} eV.

Geometric structures of the clusters were optimized from several hypothetical initial structures using an optimization algorithm called the conjugate gradient method.[32] As initial structures in the geometry optimization procedure for Na_N and Cu_N, the optimized cluster structures obtained from empirical atomic pair potentials such as Lennard-Jones, Morse, Sutton–Chen, etc.,[33] were employed along with optimized structures based on FP calculations that were obtained in previous studies.[24–26]

In addition to these structures, structures expected to exist from the experimental photoelectron spectra[34–37] and those expected to exist in the neighborhood of the local minimum points on the potential energy surface from our experience of the optimization procedures for these systems[24] were selected. The optimized structures of Na_N and Cu_N ob-

tained in this study were employed as the initial structures of Ag_N in the geometry optimization procedure, and the interatomic distances satisfying the nearest neighbor atomic distance ratio between the Na, Cu, and Ag bulk crystals were scaled.

The electronic density of states of the Na, Cu, and Ag bulk crystals were calculated for comparison with those of the clusters. The same cutoff energies and optimization method used for the cluster systems were also used for the bulk calculations. The lattice constants were optimized for the hcp and bcc structures for Na, and the fcc structure for Cu and Ag. Brillouin zone integration was carried out for the $\boldsymbol{k}$-point meshes generated by the Monkhorst–Pack scheme.[38] For the bulk bcc, fcc, and hcp structures, the number of meshes were selected to be $8\times8\times8$, $8\times8\times8$, and $8\times8\times4$, respectively. The convergence criteria of the total energy for the bulk bcc, fcc, and hcp structure were set to be within 1.0×10^{-4}, 1.0×10^{-4}, and 5.0×10^{-3} eV/atom, respectively. The nearest neighbor diatomic distances, binding energies, and bulk moduli for the dimers and bulk crystals are presented in Appendixes A and B. The Vienna *Ab-initio* Simulation Package (VASP) was employed in this study.[39]

III. CLUSTER GEOMETRIES

A. *N* dependence of most and metastable structures

In general, unlike the case of molecules, clusters have various energetically nearly degenerated metastable structures. Therefore, the metastable as well as most stable structures must be considered for understanding cluster-related phenomena.

Figures 1–3 show the most and metastable structures of the Na_N, Cu_N, and Ag_N clusters for $3\leq N\leq12$, $13\leq N\leq22$, and $34\leq N\leq75$, respectively. In these figures, the metastable structures are carefully selected to show the structural-type transition, as described below. Almost all of the most and metastable structures of Na_N, Cu_N, and Ag_N clusters are similar. Therefore, to save space, the cluster structures are represented by the structure of Cu_N in the figure. The types of these structures are classified by notations I–V. This classification obeys the order of stability in the structural type of Cu_N. The symbols *L*, *P*, *O*, and *C* after I, II, III, IV, and V indicate linear, planar, opened, and closed structures, respectively. For a detailed analysis of the correlation between the structural type and the energetical stability of the clusters, these structural types should be further classified according to the symbols. Both opened and closed structures are three dimensional. The coordination number (CN) is a necessary concept for the classification of these three-dimensional structures. Although the CN can also be defined for linear and planar structures, it is not required for the classification in this study. An opened structure is defined as one without atoms whose CNs are greater than or equal to 11. Other three-dimensional structures are defined as closed structures. The three values listed after the symbols *L*, *P*, *O*, and *C* represent the relative energies of the most stable structures of Na_N, Cu_N, and Ag_N, respectively. A value of 0.000 is assigned to the most stable structure, and the relative energies of the metastable structures are expressed in eV.

We consider the case of $N=6$ as an example. As shown in Fig. 1, the structural type of the most stable structure in Na_6 is II, while that in Cu_6 and Ag_6 is I. The structural types of the second stable structure in Na_6 are I and in Cu_6 and Ag_6, II. The structural type of the third stable structures in Cu_6 and Ag_6 is III. However, structure III is not found in Na_6. A symbol N indicates a structural type that has not been found. The two different figures of structure II show the same cluster structure viewed from different angles. Such different figures for the same structure are also shown for the other values of *N*. Structural type IV at $N=10$ corresponds to Plato's polyhedron. The numerous highly symmetric structures including Plato's polyhedron are labeled as TETRA, OCTA, ICO, CUBO, and DECA, and they represent tetrahedron, octahedron, icosahedron, cuboctahedron, and decahedron, respectively. As shown in Figs. 2 and 3 the three structures composed of blue, red, and silver spheres represent the structures of Na_N, Cu_N, and Ag_N, respectively. These structures are shown to emphasize the relatively large structural differences from the relation of similarity.

The following conclusions are obtained from the most and metastable structures of the clusters. The optimized structures of the Na_N, Cu_N, and Ag_N clusters are almost identical if the most and metastable structures are simultaneously considered. These features are restricted to the size range of $N\leq22$.[24–27] In particular, the most stable structure of the three clusters for $N\leq22$ can be identified with high probability. For $N=34$ and 38, all of the most stable structures of the three clusters are different. For $N=40$, the most stable structures of alkali and noble metal clusters clearly differ. As described later in detail, the most stable structure of Na_{40} obtained in this study is more stable than that obtained in previous studies.[40–42]

For $N=55$, all of the three different clusters favor structural type I (icosahedral structure) for their most stable structure. The second and third stable structures at $N=55$ include an atomic vacancy in an icosahedral flame.[43] For all of the three different metal clusters, these metastable structures are more stable than the higher symmetric structures such as a decahedron and cuboctahedron. Generally, it is difficult to define an atomic vacancy in a cluster because it is a system without periodicity in the structure. However, an icosahedral structure can be considered to be a structure that is cleaved from a quasicrystal. In fact, $N=55$ is the minimum number that shows an atomic vacancy stability in the cluster structure. For $N\geq55$, with increasing *N*, structures of the clusters approach the periodic bulk crystal structure. Therefore, it is expected that the probability of vacancy formation will increase in finite cluster systems.

An overview of the structural-type transition of the most stable structures in Na_N, Cu_N, and Ag_N clusters with increasing *N* is described below. The structures of Na_N, Cu_N, and Ag_N clusters are stable in a linear structure at $N=2$, planar structure at $3\leq N\leq5$ (Na), 6 (Cu and Ag), opened structure at 6 (Na), 7 (Cu and Ag) $\leq N\leq15$ (Na and Cu), 16 (Ag), and closed structure at $N\geq16$ (Na and Cu), 17 (Ag). These features were already shown in previous studies.[24–27] In this work, the quantitative classification for the shape was given for the later discussion. Systems comprising four or more

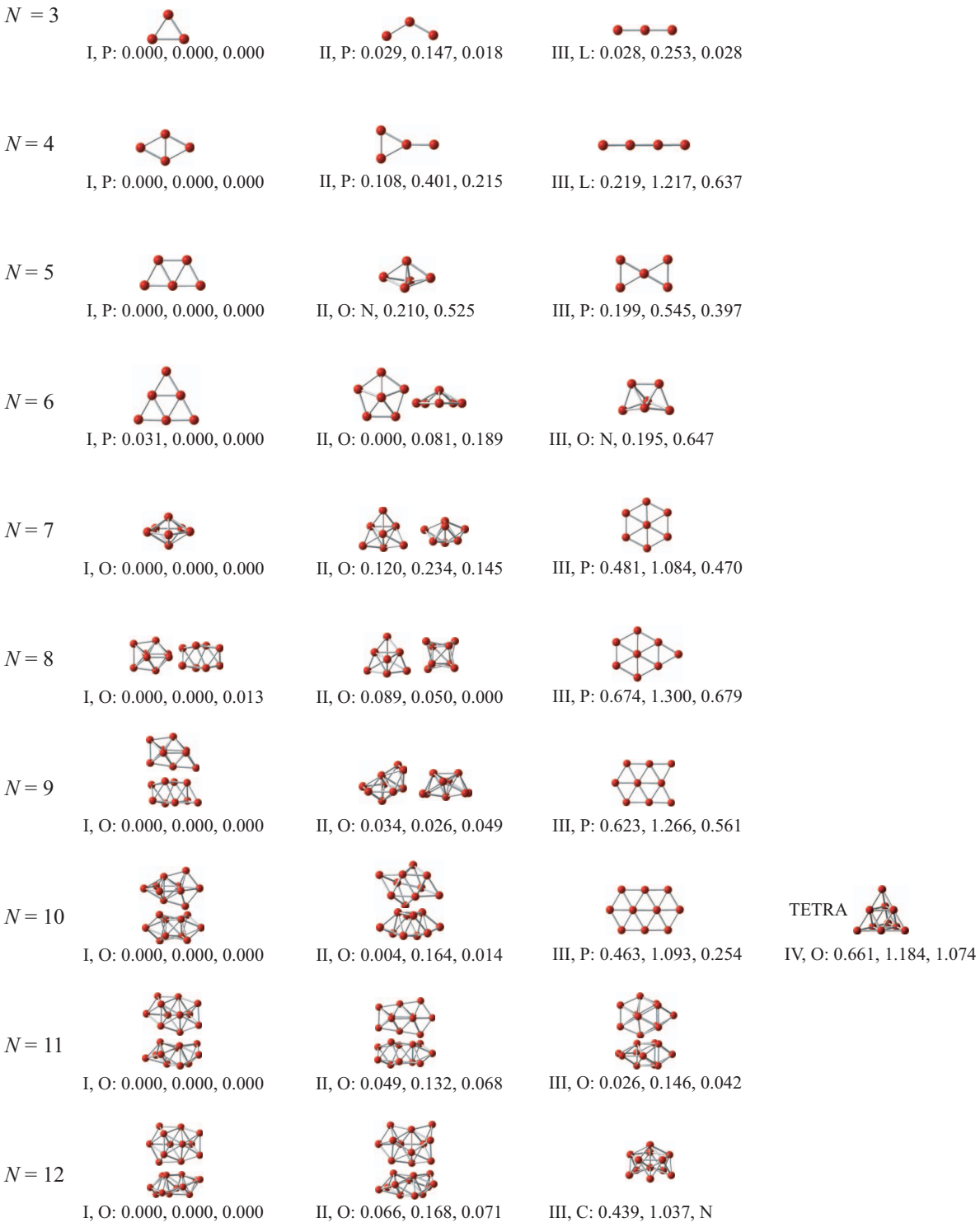

FIG. 1. The most and metastable structures of Na_N, Cu_N, and Ag_N clusters for $3 \leq N \leq 12$ are shown. Almost all of the most and metastable structures of these clusters are similar. Therefore, the cluster structures are represented by the structures of Cu_N to save space in this figure. The structures are classified according to their types using notations I–IV. This classification obeys the stability order in the structural type of Cu_N. The symbols *L*, *P*, *O*, and *C* used after the notations indicate linear, planar, opened, and closed structures, respectively. Opened and closed structures are both three-dimensional structures. An opened structure is defined as one without any atoms whose coordination number is greater than or equal to 11. Other three-dimensional structures are defined as closed structures. The three values following the symbols *L*, *P*, *O*, and *C* represent the relative total energies of the most stable structures of Na_N, Cu_N, and Ag_N, respectively. A value of 0.000 is assigned to the most stable structure and the energy of metastable structures is expressed in units of eV. The symbol *N* is used to denote a structure that cannot be identified. The two different figures shown above show views of the same cluster from different angles. The numerous, highly symmetric structures, including Plato's polyhedron, are labeled as TETRA, OCTA, ICO, CUBO, and DECA, and they represent tetrahedron, octahedron, icosahedron, cuboctahedron, and decahedron, respectively.

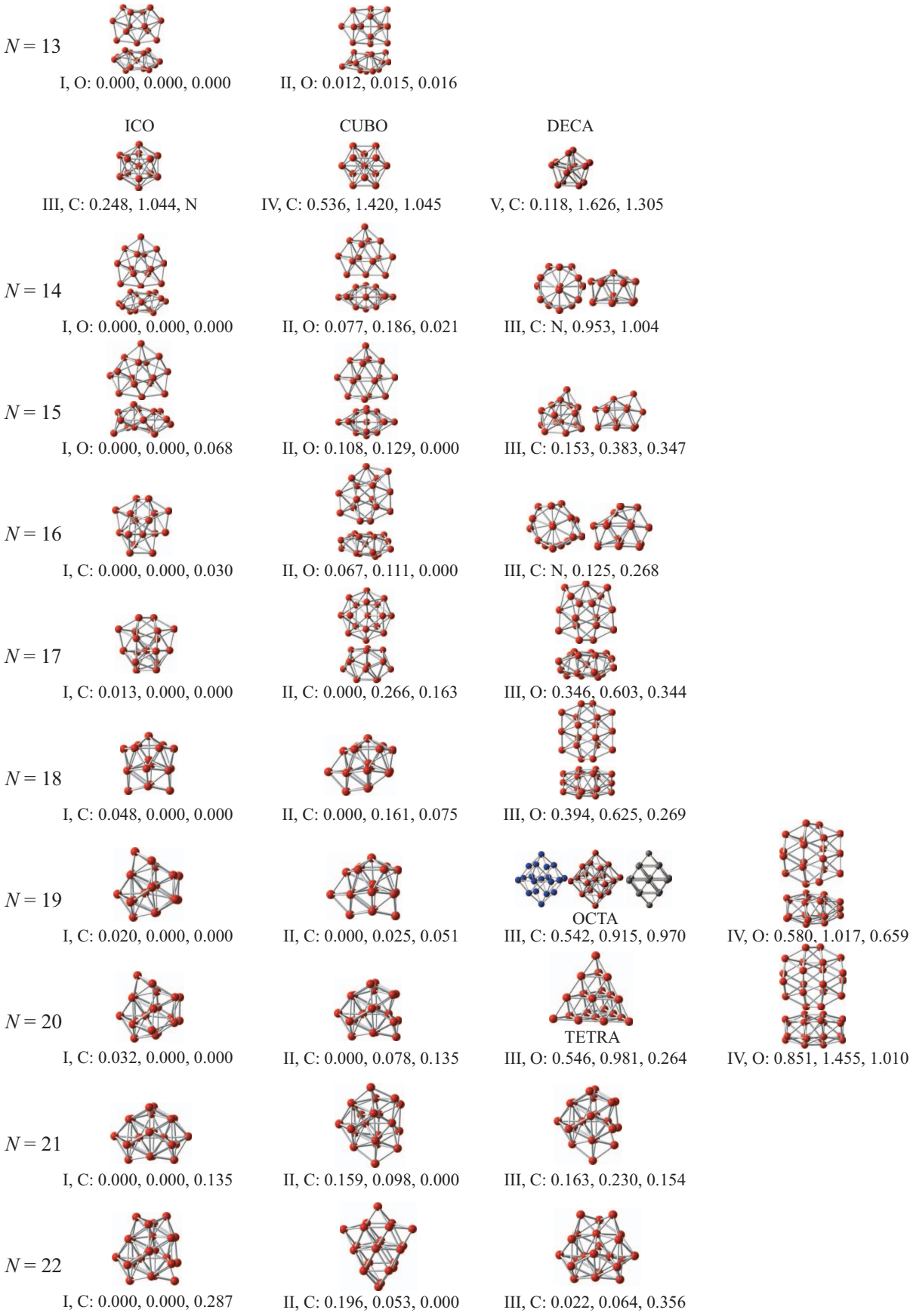

FIG. 2. The most and metastable structures of Na_N, Cu_N, and Ag_N clusters for $13 \leq N \leq 22$ are shown. The notations used are the same as those in Fig. 1. Some isomers of Na_N and Ag_N are also shown for cases where their structural deviations are relatively large from the relation of similarity. The structures of Na_N and Ag_N are indicated in blue and silver, respectively.

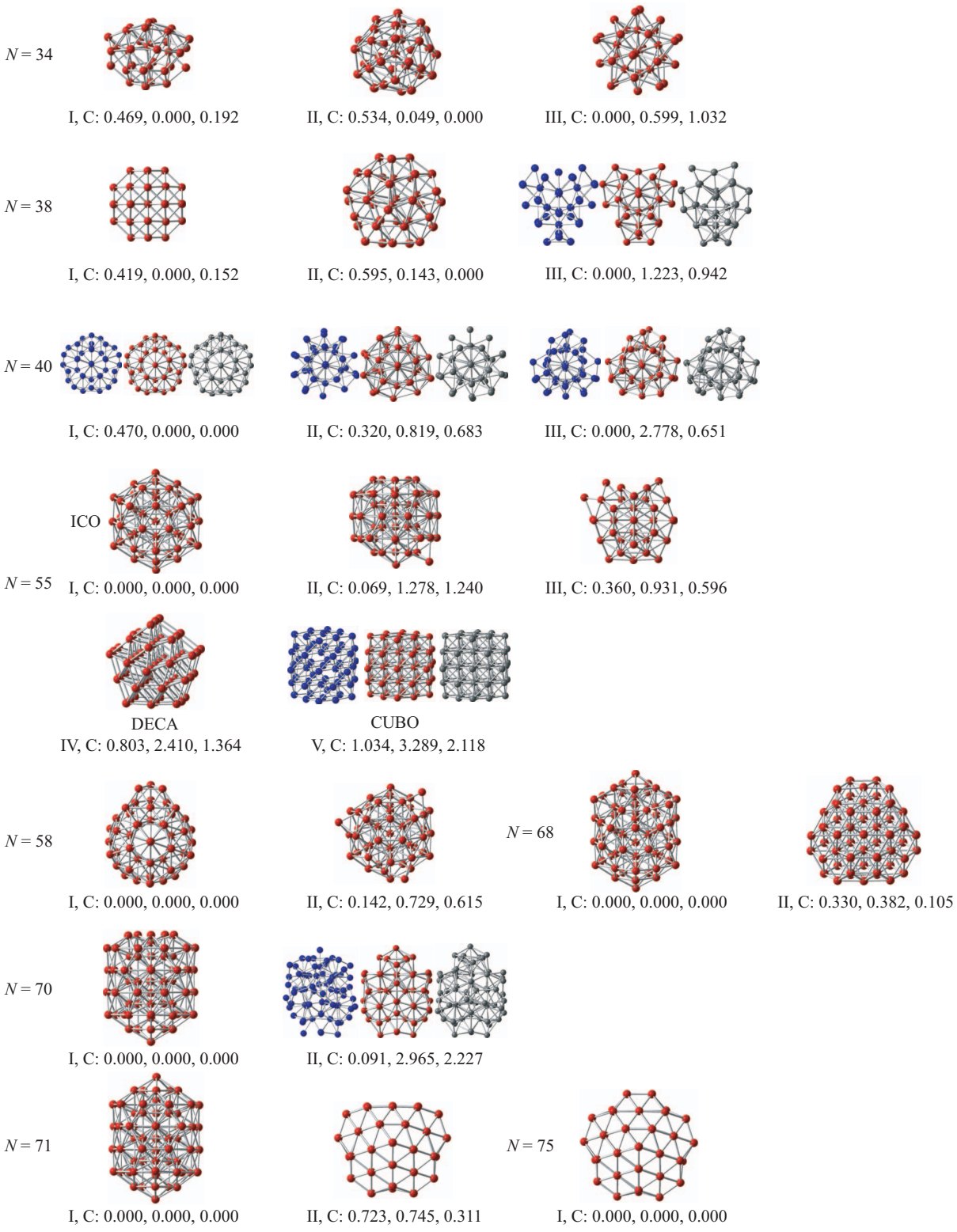

FIG. 3. The most and metastable structures of Na_N, Cu_N, and Ag_N clusters for $34 \leq N \leq 75$ are shown. The notations used are the same as those in Figs. 1 and 2.

atoms can possibly assume three-dimensional structures such as a tetrahedron and trigonal pyramid. However, for all of the three different metal clusters, the most stable structures are not three dimensional at $4 \leq N \leq 5$ (Na), 6 (Cu, and Ag). At $N=4$, the three-dimensional structures are not stable for these systems. Instead, a rhombus structure is stable at $N=4$. A three-dimensional structure such as a tetrahedron is realized in other metal clusters such as Mg_4.[44]

The stable cluster structures obtained for small size range $N \leq 22$ in this study can be roughly understood from knowledge of the electronic states using the spherical jellium model (SJM). The main difference between the FP model used in this study and the SJM is the manner in which the atomic configuration in the cluster is treated. In the SJM, only the outermost valence electrons in the each atom composing the cluster are considered as valence electrons. The

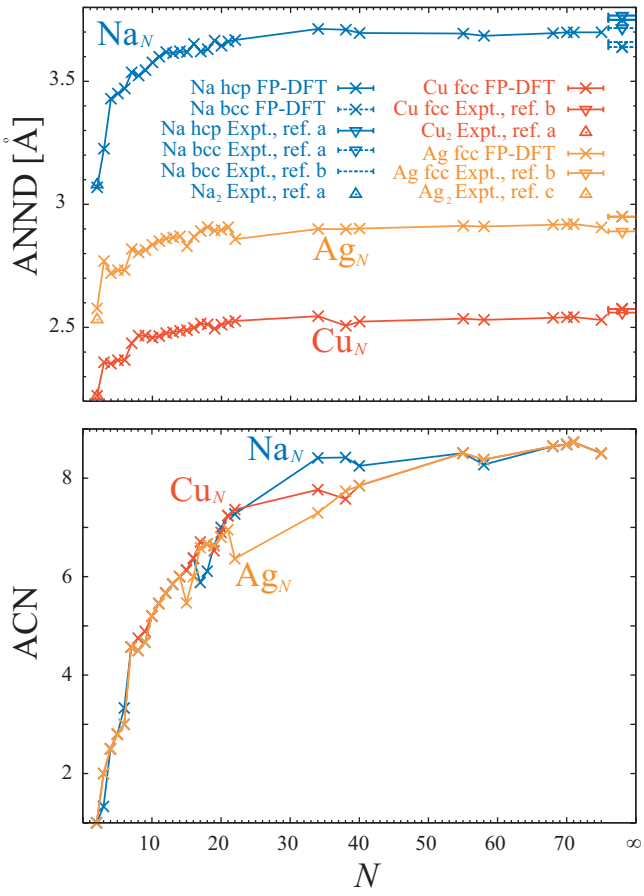

FIG. 4. (a) shows the N dependence of the ANND in units of angstroms and (b) shows the ACN from atom to bulk for Na_N, Cu_N, and Ag_N for $1 \leq N \leq 75$, and ∞ (bulk). The ACN values of the bulk crystal—12 (Na: hcp, Cu: fcc, Ag: fcc) and 8 (Na: bcc), are not shown in (b). References a, b, and c, correspond to Refs. 46–48, respectively.

other electrons and nuclei are unified into a uniform positive charge distribution with a spherical surface boundary. Therefore, the valence electrons in the SJM reside in the central force field. As a result, each degenerated valence electronic state is specified with a monoangular momentum: S,P,D,F,…, in a manner similar to the case of electrons in an atom, and protons and neutrons in a nucleus. The stable structures of the metal cluster obtained in this study for small size range $N \leq 22$ can be roughly considered as those satisfying the cluster shapes followed by the valence electronic density distribution that originates from the occupied orbitals in the SJM. For larger size range $N \geq 34$, the shapes are not simply explained from the knowledge.

B. *N* dependence of the averaged nearest neighbor distance and coordination number

Figure 4(a) shows the averaged nearest neighbor distance (ANND) of the most stable structures of Na_N, Cu_N, and Ag_N clusters for $2 \leq N \leq 75$. ANND is defined as the sum of the nearest neighbor atomic distances divided by the number of bonds in a cluster. In this study, the nearest neighbor atom is defined as atom which resides in space from the center of noted atom within 4.2168, 3.1488, and 3.6072 Å for Na_N, Cu_N, and Ag_N, respectively. As shown in the figure, the ANND value of the cluster reaches approximately 90% of the bulk value at $N=20$ for all of the three different clusters. However, the ANND does not converge to the bulk value at $N=75$, and the values are approximately 98% of the bulk ones. Over the entire range of N, the ratio of ANND among the three different clusters agrees well with that of the bulk crystals.

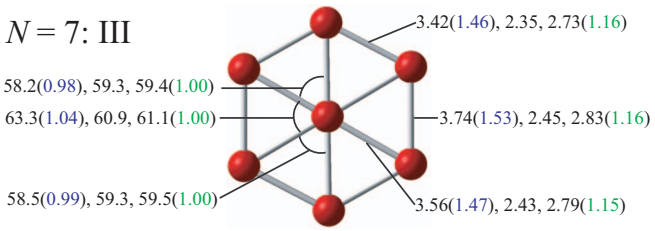

FIG. 5. The deviation from the relation of similarity shown in structure III of Na_7, Cu_7, and Ag_7 shown in Fig. 1. The values of the angles and interatomic distances are shown in the order of Na_7, Cu_7, and Ag_7. Structure III of Cu_7 is shown as an example. The angles and interatomic distances are expressed in units of degrees and angstroms, respectively. The blue and green values in the parentheses represent the relative ratio of angle(distance)$_{Na_7}$/angle(distance)$_{Cu_7}$ and angle(distance)$_{Ag_7}$/angle(distance)$_{Cu_7}$, respectively.

Figure 4(b) shows the averaged coordination number (ACN) of the most stable structures of Na_N, Cu_N, and Ag_N clusters over the range of $2 \leq N \leq 75$. ACN is defined as the sum of the nearest neighbor coordinated atomic number for all atoms composing the cluster divided by N. The N dependence of ACN for the three different clusters is similar; it should be noted that the ACN values do not reach 9 (75% of the bulk value of 12) even at $N=75$. This is attributable to the existence of a surface in the cluster.

C. Difference between planar structures of sodium, copper, and silver clusters

As described in Sec. III A, the most and metastable structures of the three different metal clusters are quite similar. Here, the cluster structures having the same structural type are compared quantitatively using structure III at $N=7$ as an example. Figure 5 shows the details of the structures, represented by the Cu_7 structure as an example. The three values represent the angle or interatomic distance of Na_7, Cu_7, and Ag_7, respectively. These values are expressed in degrees or angstroms, respectively. The blue and green values in parentheses represent the relative angle ratios: angle(distance)$_{Na_7}$/angle(distance)$_{Cu_7}$ and angle(distance)$_{Ag_7}$/angle(distance)$_{Cu_7}$, respectively.

Structure III in Na_7 belongs to the C_{2h} point group, while in Cu_7 and Ag_7, it belongs to the D_{2h} point group; all of these structures are third stable structures. These structures have a Jahn–Teller deformation[45] in the equilateral hexagon in the D_{6h} point group. As expected, the relative angle ratio of Ag_7 is closer to 1 than that of Na_7. This is a typical example that indicates the stronger similarity between the two noble metal clusters. However, there are several exceptions in clusters having a larger value of N. This may occur due to the increase in the number of degrees of freedom in the atomic positions. Therefore, it is not possible to present an oversimplified picture of the degree of similarity in these cluster structures.

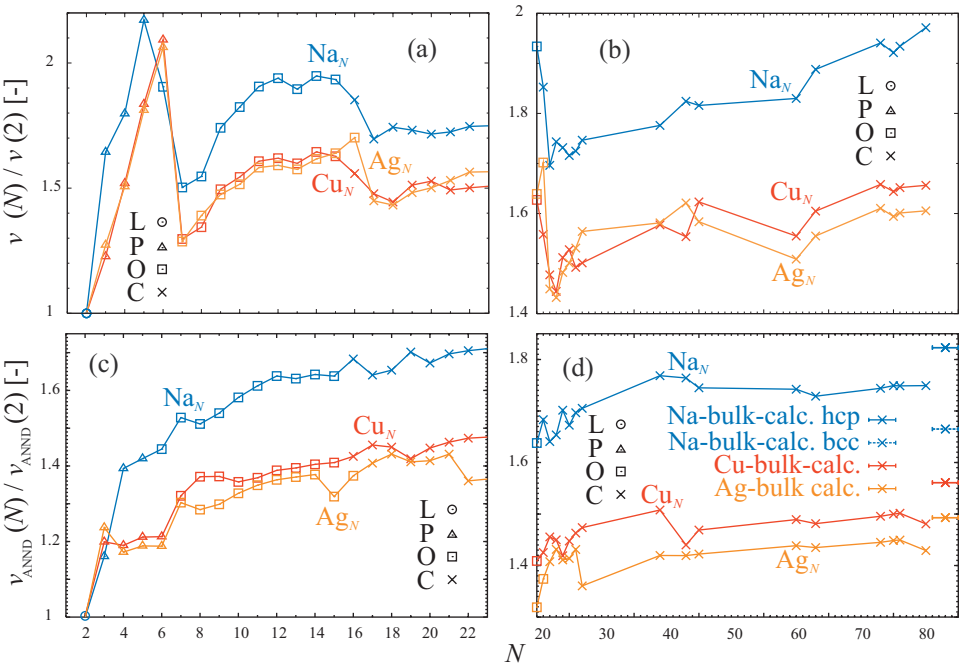

FIG. 6. (a), (b), (c), and (d) show the N dependence of the normalized specific cluster atomic volume $v(N)/v(2)$, and the normalized cluster atomic volume $v_{ANND}(N)/v_{ANND}(2)$ for the most stable structures of Na_N, Cu_N, and Ag_N for $2 \leq N \leq 22$ and $15 \leq N \leq 75$, respectively. Each structure is denoted using the symbols L, P, O, and C.

D. *N* dependence of the specific atomic volume

One of the specific atomic volume of cluster $v(N)$ can be defined as

$$v(N) \equiv \frac{4}{3}\pi\langle R\rangle^3/N. \tag{1}$$

Here, $\langle R\rangle$ indicates the averaged distance between each atomic coordination $\boldsymbol{R}_i$ and center of mass $\boldsymbol{R}_{\mathrm{CM}}$ in a cluster. In other words, $\langle R\rangle$ is given as

$$\langle R\rangle = \frac{1}{N}\sum_{i=1}^{N} |\boldsymbol{R}_i - \boldsymbol{R}_{\mathrm{CM}}|. \tag{2}$$

It should be noted that the specific volume does not converge to the true atomic volume for the infinite lattice. To compare the N dependence of $v(N)$ for the different metal clusters, each $v(N)$ is normalized to that of a dimer, i.e., $v(2)$.

Figure 6(a) shows the N dependence of a normalized volume for the most stable structures of Na_N, Cu_N, and Ag_N for $2 \leq N \leq 22$. The N dependence of the normalized volume $v(N)/v(2)$ is very similar in the three metal clusters. The trends of the change in the N dependence at transition sizes N between different structural types are indicated using the symbols L, P, O, and C. $v(N)/v(2)$ decreases significantly at N from P to O. Further, significant decreases are observed at N from O to C.

Figure 6(b) shows the volumes of the most stable structures in the range of $15 \leq N \leq 75$. Here, the scale of $v(N)/v(2)$ is expanded to show the change clearly. In general, for $N \geq 20$, $v(N)/v(2)$ increases monotonically with N for all of the three metal clusters. However, it should be noted that the values decrease significantly with increasing N between Cu_{40} (Ag_{40}) and Cu_{55} (Ag_{55}), unlike the case of Na_{40} and Na_{55}. This can be attributed to the effect of d electrons in that they may shrink the interatomic distances of the quasispherical structure—an icosahedron which is the most stable structure at $N=55$. The relation with the melting point T_m is discussed in Appendixes A and B.

The cluster volume cannot be defined in unique. Here, another cluster volume is defined based on the ANND. If a cluster is supposed to be an assemble of rigid atomic spheres with half of ANND radius, the atomic volume in cluster $v_{ANND}(N)$ is defined as below,

$$v_{ANND}(N) \equiv \frac{4}{3}\pi\left(\frac{\mathrm{ANND}}{2}\right)^3. \tag{3}$$

Figures 6(c) and 6(d) show the N dependence of the normalized atomic volume $v_{ANND}(N)/v_{ANND}(2)$. It is apparent that the drastic change in the trend of N dependence in $v_{ANND}(N)/v_{ANND}(2)$ is not observed for the three metal clusters.

IV. *N* DEPENDENCE OF THE CALCULATED CLUSTER ENERGY FOR $2 \leq N \leq 75$ AND ∞

A. Overall aspects of the cluster binding energy

As described in Sec. III A, the most stable structures of the three metal clusters were searched over the range of $2 \leq N \leq 75$ and the ground state cluster energies $E(N)$ were evaluated. In general, it was observed that $E(N)/N$ of the metal clusters increased with N and approached $E(\infty)/\infty$, which corresponds to the value of the bulk cohesive energy. Interestingly, $E(N)$ exhibited higher or lower values at a particular value of N. To investigate the aspects of $E(N)$ in detail, the N dependence of the difference between $E(N)$ and the liquid drop model[11] (LDM) average $\langle E(N)\rangle$, defined as

$$\delta E(N) \equiv \langle E(N)\rangle - E(N), \tag{4}$$

is evaluated. Here, $\langle E(N)\rangle$ is expressed by a linear combination of three terms as shown below,

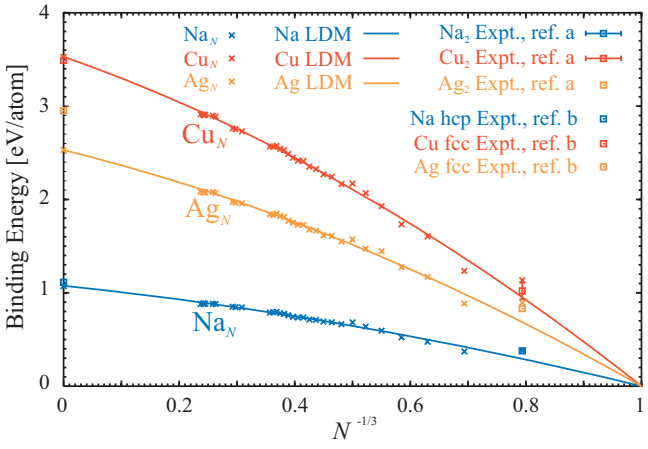

FIG. 7. The dependence of the binding energy of the ground state structures of Na_N, Cu_N, and Ag_N $[1 \leq N \leq 75, \infty$ (bulk)] on $N^{-1/3}$. For each element, the LDM average is also shown. References a and b correspond to Refs. 46 and 47, respectively.

$$\langle E(N) \rangle = a_v N + a_s N^{2/3} + a_c N^{1/3}. \tag{5}$$

The first, second, and third terms denote the volume, surface, and curvature energy, respectively. The fitting parameters a_v, a_s, and a_c were determined as described below. Here, the averaged cluster binding energy per atom $\langle E_b(N) \rangle / N$, defined as

$$\langle E_b(N) \rangle / N \equiv E(1) - \langle E(N) \rangle / N, \tag{6}$$

must be calculated to evaluate $\delta E(N)$.

a_v was uniquely determined from the cohesive energy of the bulk crystal that corresponds to $\langle E_b(N) \rangle / N$ at $N=\infty$. a_s and a_c were determined as coefficients of the fitting curve $\langle E_b(N) \rangle / N$ to the cluster binding energy $E_b(N)/N$ over the range of $2 \leq N \leq 75$ by applying the least-squares method and minimizing those values under the boundary condition $\langle E_b(1) \rangle = 0$. Figure 7 shows the cluster binding energy per atom $E_b(N)/N$ and the LDM average $\langle E_b(N) \rangle / N$ as functions of $N^{-1/3}$. $E_b(N)/N$ and the average $\langle E_b(N) \rangle / N$ of Na_N, Cu_N, and Ag_N at $N=2-75$ and ∞ are presented. $N^{-1/3}=0$, 0.237, and 0.794 correspond to $N=\infty$, 75, and 2, respectively.

We now consider the difference between $E_b(N)/N$ and the LDM average $\langle E_b(N) \rangle / N$. With an increasing in N from 2 to 75 and then ∞, a significant similarity is observed in the difference among the Na_N, Cu_N, and Ag_N clusters in which each element has one s electron in the outermost shell. For the sake of comparison, the experimental bulk cohesive energy and binding energy of a dimer[46–48] are also shown in Fig. 7. The values of the bulk cohesive energy and binding energy obtained through our calculations and experiments are in good agreement. However, in a Ag bulk crystal, the calculated cohesive energy does not agree well with the experimental value. This disagreement may be attributable to the incompleteness of the description of the Ag ($Z=47$) atom. As reported in previous studies,[49] the disagreement originates from the treatment method of the relativistic effect through the pseudopotential, the exchange-correlation energy functional—GGA, and the basis set for the electrons—plane waves. Although an improvement in the description is desired, we expect that the qualitative feature of the growth behavior of a Ag cluster from an atom to bulk shown in this study will not change.

B. Detailed analysis of the *N* dependence of cluster binding energy

In Sec. IV A, a strong similarity is pointed out for Na_N, Cu_N, and Ag_N clusters in the N dependence of the difference between the cluster binding energy per atom $E_b(N)/N$ and the LDM average $\langle E_b(N) \rangle / N$. In this section, we analyze this similarity in detail.

Figure 7 shows that the difference for each of the three clusters approaches 0 with increasing N. However, it is difficult to compare them for large value of N. Therefore, the N dependence of the N multiplied values $\delta E(N) \equiv -E(N) + \langle E(N) \rangle$ is noted for the detailed analysis.

Figures 8(a) and 8(b) show the N dependence of $\delta E(N)$ for the three metal clusters over the ranges $1 \leq N \leq 22$ and $15 \leq N \leq 75$, respectively. In Fig. 8(a), a strong similarity is observed in the N dependence of $\delta E(N)$ for $1 \leq N \leq 22$. These values indicate an odd-even alternation in N. In other words, $\delta E(N)$ increases from an odd N to the next even N, and then decreases from an even N to the next odd N. In many cases, $\delta E(N)$ is positive at even N and negative at odd N. In Fig. 8(b), a significant similarity is observed in the N dependence of $\delta E(N)$ for $15 \leq N \leq 75$. $\delta E(N)$ is larger at $N=34$, 55, and 58 and smaller at $N=40$, 68, 70, 71, and 75 are compared to those at the neighborhood N considered in this study. The amplitudes of $\delta E(N)$ for Cu_N and Ag_N are much larger than that for Na_N. Further, the values of Cu_N and Ag_N are closer. This is attributable to the effect of d electrons in noble metal clusters.

C. Definition of the cluster magic number and identification

In many previous studies of clusters, a N value that gives a special cluster stability has been frequently called as the magic number. To understand the N-dependent system stability, it is necessary to evaluate the magic number based on FP calculations because it can be a standard magic number. However, criterion of the magic number has not yet been presented. Therefore, to understand the N-dependent system stability, we must first define the magic numbers.

First, the curvature of the cluster energy for $N-\Delta_2 E(N)$, defined as

$$\Delta_2 E(N) \equiv E(N+1) + E(N-1) - 2E(N), \tag{7}$$

is discussed. If $\Delta_2 E(N)$ exhibits a positive value at N, namely,

$$\Delta_2 E(N) \geq 0, \tag{8}$$

N may be a magic number because $E(N)$ might be a local minimum for N. Figure 8(c) shows the N dependence of $\Delta_2 E(N)$ for the three metal clusters. Here, the magic numbers of the three clusters can be identified as $N=2$, 4, 6 (Na, Ag), 8, 10, 12, 14, 18, and 20. For these values of N, an odd-even alternation is clearly observed. All of these values of N are even numbers and it is natural to consider that the odd-even

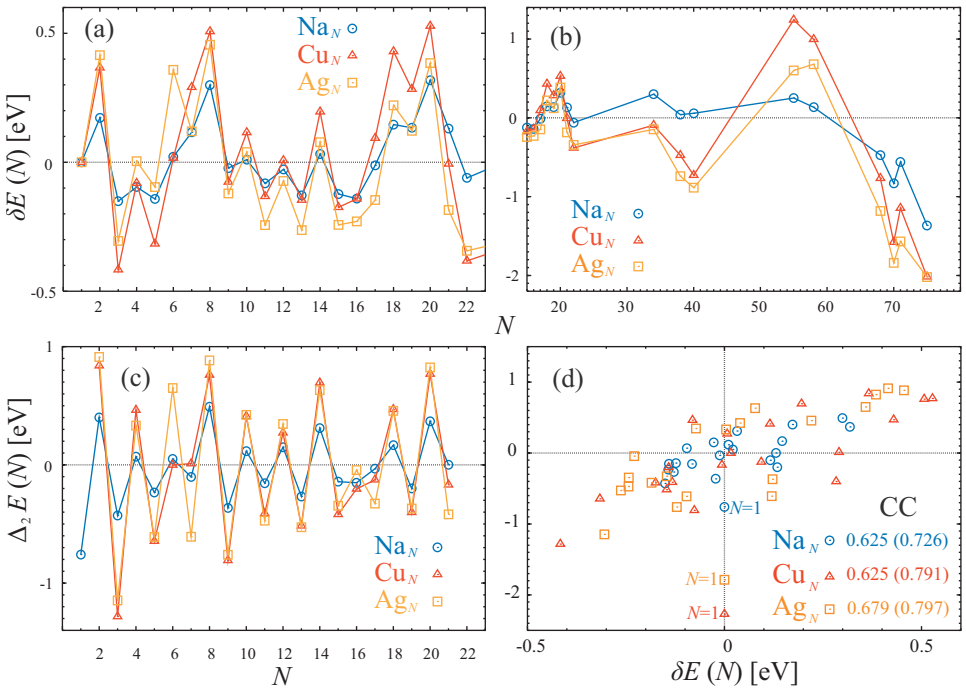

FIG. 8. (a) and (b) show the N dependence of $\delta E(N)$ for the most stable structures of Na_N, Cu_N, and Ag_N clusters at $1 \leq N \leq 22$ and $15 \leq N \leq 75$, respectively. (c) shows $\Delta_2 E(N)$ for the most stable structures of Na_N, Cu_N, and Ag_N at $1 \leq N \leq 21$. (d) shows correlation between and $\Delta_2 E(N)$ for Na_N, Cu_N, and Ag_N at $1 \leq N \leq 21$. The CCs for them are also shown. The numbers in parentheses mean the CCs for them at $2 \leq N \leq 21$.

alternation originates from the spin degeneracy and each electronic shell closing in the clusters as presented in the curvature of eigenvalue sum within the Hückel model.[50] In addition, the N dependences of the peak intensities are similar in the three clusters, although the absolute values of the peaks are larger in the noble metal clusters than in the alkali metal cluster for most values of N. As in the case of $\delta E(N)$ described in Sec. IV B, the values of $\Delta_2 E(N)$ are closer in the noble metal clusters.

Although it is possible to derive other conclusions from the absolute values of $\Delta_2 E(N)$, only $\Delta_2 E(N)$ may not be a sufficient criterion for the evaluation of magic numbers. In general, additional information is required for the identification.

$\delta E(N)$ can be a criterion for identifying magic numbers because of its definition: the energy difference between a real cluster and the continuously averaged energy model, LDM. The magic numbers N should satisfy the condition

$$\delta E(N) \geq 0. \tag{9}$$

This condition is satisfied for N=2, 4 (Ag), 6, 7, 8, 10, 12 (Cu), 14, 17 (Cu), 18, 19, 20, and 21 (Na).

If only $\Delta_2 E(N)$ and $\delta E(N)$ are considered, magic numbers N can be defined as

$$\Delta_2 E(N) \geq 0, \quad \delta E(N) \geq 0. \tag{10}$$

If this criterion is employed for the magic numbers in Na_N, Cu_N, and Ag_N clusters for $N \leq 21$, the common magic numbers N=2, 4 (Ag), 6, 8, 10, 12, 14, 18, and 20 are identified.

It should be noted that the set of magic numbers evaluated from $\Delta_2 E(N)$, and $\delta E(N)$ for $1 \leq N \leq 21$ is similar. As shown in Fig. 8(d), there are strong positive correlations between $\delta E(N)$ and $\Delta_2 E(N)$. The correlation coefficients (CCs) between them for Na_N, Cu_N, and Ag_N are 0.625, 0.625, and 0.679, respectively. The CCs for $2 \leq N \leq 21$ are larger; CCs for Na_N, Cu_N, and Ag_N are 0.726, 0.791, and 0.797, respectively. These differences can be attributed to the definition of $\delta E(1)$, and the large minus value of $\Delta_2 E(1)$s. These large CCs suggest that the $\delta E(N)$ only itself can be a good criterion of the magic number.

In this study, $\Delta_2 E(N)$ for $N \geq 34$ is not evaluated. For $N \geq 34$, magic numbers are identified only from $\delta E(N)$. Therefore, N=34 (Na), 38 (Na), 40 (Na), 55, and 58 are identified as magic numbers. In this definition, the odd number N=55 is also considered to be a magic number.

In our FP calculations, the common feature of the magic numbers in Na_N, Cu_N, and Ag_N can be attributed to the delocalized s valence electrons. The localized d electrons in the noble metal clusters increase the stability difference between magic and not-magic clusters.

D. *N*-dependent stability of Na_N clusters from the experiment and total energy calculations

1. $\Delta_2 E(N)$

The N dependence of the peak intensity $I(N)$ in the experimentally observed abundance spectra and the cluster energy $E(N)$ evaluated from the FP calculations have not yet been compared quantitatively. This comparison is important for understanding the magic number observed in the experiment. On the basis of several assumptions, semiquantitative comparison method[17,20] has already been developed for an experimental result of Na_N (Ref. 3) and the theoretical total energy calculations. Although experimental results for Cu_N and Ag_N (Refs. 51 and 52) are available, they cannot be easily compared with our calculation results quantitatively. Therefore, in this section, we only focus on the magic numbers of Na_N.

With regard to experiments with Na_N, only the result of Knight *et al.*[3] is discussed. As shown in other experiments with Na_N such as those by Bjørnholm *et al.*,[13] Rabinovitch *et al.*,[53] etc., main peaks were also observed at N=8, 20, 40, 58,

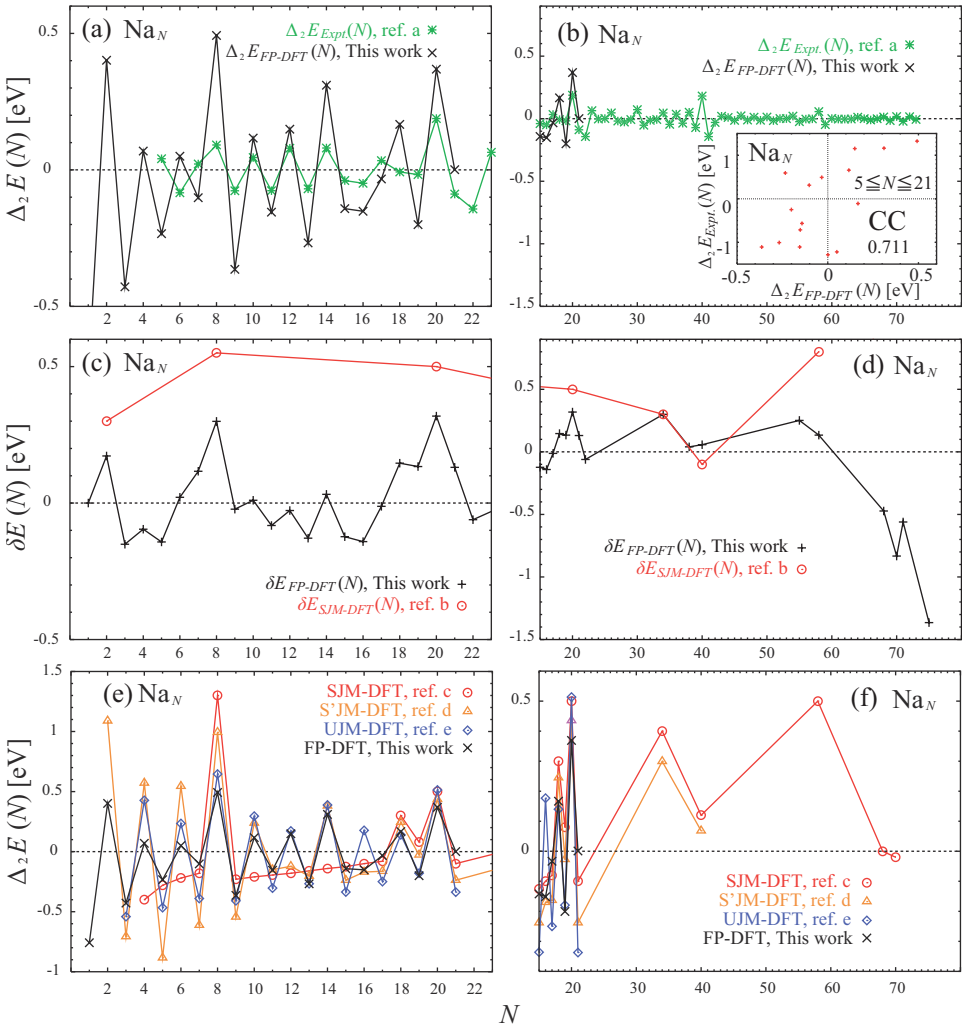

FIG. 9. (a) and (b) show the N dependence of $\Delta_2 E(N) = k_B T \ln([I(N)^2]/[I(N+1)I(N-1)])$ of Na_N as given by Knight *et al.* (Ref. a corresponds to Ref. 3) at 700 kPa Ar in the cluster production step, and $\Delta_2 E(N)$ of the FP model for Na_N clusters at $1 \leq N \leq 22$ and $15 \leq N \leq 75$, respectively. For $\Delta_2 E(N)$ value given by Knight *et al.*, the value of the temperature is set to 800 K as measured in the nozzle channel before the cooling step in the experiment. The inset of (b) shows correlation in $\Delta_2 E(N)$ evaluated from the FP model and the experiment for Na_N at $5 \leq N \leq 21$. (c) and (d) show the N dependence of $\delta E(N)$ of the SJM (Ref. 14) and FP model. (e) and (f) show the N dependence of $\Delta_2 E(N)$ of Na_N clusters evaluated by various jellium models and the FP model for $1 \leq N \leq 22$ and $15 \leq N \leq 75$, respectively. References c, d, and e, correspond to Refs. 6, 55, and 8, respectively.

and 92. Therefore, without significant improvements in the experimental method, these abundance spectra and magic numbers appear to remain unchanged. Obviously, if the experimental results remain unchanged, the theory itself must be reconsidered.

Here, the curvature of $E(N)$ evaluated from our calculations and the peak intensity $I(N)$ in the abundance spectra were semiquantitatively compared based on the method described below. The abundance spectra of Na_N clusters reported by Knight *et al.* are considered to be attributed as follows. First, Na atomic vapor is formed by heating Na bulk solid in an Ar-gas-filled closed space in the experimental apparatus.[54] Then, Na_N clusters are formed by the adiabatic cooling of the mixture after passing through the skimmer in the apparatus. Then, N-distributed neutral charged Na_N clusters were assumed to be obtained in a thermal equilibrium condition. If the assumption for the Na_N distribution is true, the relationship

$$\rho(N) = A \exp\left(-\frac{E(N)}{k_B T}\right) \tag{11}$$

must be satisfied. Here, the $\rho(N)$, A, k_B, and T denote the number density of neutral charged Na_N, a constant, Boltzmann constant, and the absolute temperature, respectively. These clusters were ionized by light and then accelerated by an electric field for mass selection. In these steps, the N-distribution of $\rho(N)$ is assumed to remain unchanged. Finally, these clusters were detected and the N-distribution of the neutral charged clusters was observed using the detector. Therefore, finally,

$$I(N) = B\rho(N) \tag{12}$$

holds. Here, B is a constant. From Eqs. (7), (11), and (12), the following equation is derived:

$$\Delta_2 E(N) = k_B T \ln \frac{I(N)^2}{I(N+1)I(N-1)}. \tag{13}$$

Namely, $\Delta_2 E(N)$ can be evaluated from $I(N)$ of the experimental abundance spectra.

Figures 9(a) and 9(b) show the N dependence of $\Delta_2 E(N)$ evaluated experimentally by Knight *et al.*, $\Delta_2 E_{\text{expt}}(N)$, and by the FP calculations in this study, $\Delta_2 E_{\text{FP-DFT}}(N)$ for $N \leq 22$ and $15 \leq N \leq 75$, respectively.

We first compare the N dependence of $\Delta_2 E_{\text{expt}}(N)$ and $\Delta_2 E_{\text{FP-DFT}}(N)$ for neutral charged Na_N clusters. Generally, there is a good agreement between them. However, contrasting trends are observed in two rows of N: (1) $N=5$, 6, and 7 and (2) $N=17$ and 18. The peak intensity of $\Delta_2 E_{\text{expt}}(N)$ and $\Delta_2 E_{\text{FP-DFT}}(N)$ is relatively strong at $N=8$ and 20. As shown

in the inset of Fig. 9(b), large CC: 0.711 is obtained for $5 \leq N \leq 21$. For $N \geq 34$, $\Delta_2 E_{\text{FP-DFT}}(N)$ is not evaluated in this study.

As shown in Fig. 8(d), there is a strong correlation in the N dependence between $\Delta_2 E_{\text{FP-DFT}}(N)$ and $\delta E_{\text{FP-DFT}}(N)$ for Na_N. From this similarity, instead of the $\Delta_2 E_{\text{FP-DFT}}(N)$, the $\delta E_{\text{FP-DFT}}(N)$ can be considered as a comparative value to the $\Delta_2 E_{\text{expt}}(N)$. This aspect is discussed in Sec. IV D 2.

2. $\Delta_2 E(N)$ and $\delta E(N)$

The $\delta E(N)$ evaluated from the FP calculations in this study, $\delta E_{\text{FP-DFT}}(N)$, and from the DFT-based SJM calculations by Genzken and Brack,[14] $\delta E_{\text{SJM-DFT}}(N)$, are shown in Figs. 9(c) and 9(d).

In a manner similar to $\Delta_2 E_{\text{FP-DFT}}(N)$, $\delta E_{\text{FP-DFT}}(N)$ exhibits good agreement with $\Delta_2 E_{\text{expt}}(N)$ with regard to the N dependence. However, in a manner similar to the case of $\Delta_2 E_{\text{FP-DFT}}(N)$, $\delta E_{\text{FP-DFT}}(N)$ exhibits a different N dependence with $\Delta_2 E_{\text{expt}}(N)$ in two rows of N: (1) $N=5$ and 6 and (2) $N=17$ and 18. Here, it should be noted that the order of peak intensity at $N=8$ and 20 of $\delta E_{\text{FP-DFT}}(N)$ exhibits better agreement with $\Delta_2 E_{\text{expt}}(N)$ than with $\Delta_2 E_{\text{FP-DFT}}(N)$. Based on these results, $\delta E_{\text{FP-DFT}}(N)$ is compared to $\Delta_2 E_{\text{expt}}(N)$ for $N \geq 34$. Here, it is assumed that there is a similarity between the N dependence of $\delta E_{\text{FP-DFT}}(N)$ and that of $\Delta_2 E_{\text{FP-DFT}}(N)$ for $34 \leq N \leq 58$.

In $\Delta_2 E_{\text{expt}}(N)$, distinctive peaks are formed at $N=40$ and 58. Similar to the case of $\Delta_2 E_{\text{expt}}(N)$, $\delta E_{\text{FP-DFT}}(N)$ is relatively large at $N=58$. However, $\delta E_{\text{FP-DFT}}(N)$ at $N=40$ is not particularly so distinctive. Although $\Delta_2 E_{\text{expt}}(N)$ is remarkably distinctive at $N=40$, the value of $\delta E_{\text{FP-DFT}}(40)$ is not so distinctive as same as that of $\delta E_{\text{FP-DFT}}(38)$. Further, for $N=34$ and 55, $\delta E_{\text{FP-DFT}}(N)$ exhibits distinctive peaks and these values are larger than $\delta E_{\text{FP-DFT}}(40)$ and $\delta E_{\text{FP-DFT}}(58)$. In addition, for $N=68$, 70, 71, and 75, $\delta E_{\text{FP-DFT}}(N)$ has negative values, and these features are not exhibited by $\Delta_2 E_{\text{expt}}(N)$.

As shown here for Na_N, although the N dependence of $\delta E_{\text{FP-DFT}}(N)$ exhibits good agreement with that of $\Delta_2 E_{\text{expt}}(N)$ in the range of $N \leq 22$, the same is not necessarily true in the range of $N \geq 34$. This point is discussed in Sec. IV E.

E. Improvement of the magic number description for Na_N clusters within density functional calculations

In this section and Sec. IV F we evaluate the source of this disagreement in the N dependence of $\delta E(N)(\Delta_2 E(N))$ obtained from theoretical total energy calculations and $\Delta_2 E(N)$ obtained from the experiment. In this subsection, we review the N-dependent system stability of Na_N by the improvement of theoretical models.

As shown in Figs. 9(c) and 9(d), $\delta E_{\text{SJM-DFT}}(N)$ obtained by Genzken and Brack[14] exhibits a N dependence similar to that of $\delta E_{\text{FP-DFT}}(N)$ for $2 \leq N \leq 58$. Further, from Figs. 9(c)–9(f), it can be also said that the N dependence of $\Delta_2 E_{\text{SJM-DFT}}(N)$ is similar to that of $\delta E_{\text{SJM-DFT}}(N)$ over the range of $2 \leq N \leq 58$, in a manner similar to the case of $\delta E_{\text{FP-DFT}}(N)$ and $\Delta_2 E_{\text{FP-DFT}}(N)$ for $1 \leq N \leq 22$. However, the N dependence of $\delta E_{\text{FP-DFT}}(N)$ exhibits a better agreement with that of $\Delta_2 E_{\text{expt}}(N)$ for $N=34$, 40, and 58 as compared to that of $\delta E_{\text{SJM-DFT}}(N)$. This result suggests that the consideration of the explicit ionic configuration in the total energy calculation is significant to realize a better agreement with the experiment with regard to the N-dependent system stability of Na_N.

Figures 9(e) and 9(f) show the N dependence of $\Delta_2 E(N)$ for Na_N evaluated from various DFT-based models such as the SJM (SJM-DFT) by Chou *et al.*,[6] spheroidal jellium model (S'JM-DFT) by Ekardt and Penzar,[55] ultimate jellium model (UJM-DFT) by Koskinen *et al.*,[8] and the FP model (FP-DFT) in this study for $1 \leq N \leq 22$ and $15 \leq N \leq 75$, respectively. These $\Delta_2 E(N)$ values are denoted as $\Delta_2 E_{\text{SJM-DFT}}(N)$, $\Delta_2 E_{\text{S'JM-DFT}}(N)$, $\Delta_2 E_{\text{UJM-DFT}}$, and $\Delta_2 E_{\text{FP-DFT}}(N)$, respectively. The various jellium models are different from the FP calculations in the treatment of the ionic configuration and the exchange-correlation energy.

As shown in Figs. 9(e) and 9(f), all of the calculation results exhibit distinctive peaks at $N=8$, 18, and 20. In these figures, remarkable differences are obtained in the number of peaks between $\Delta_2 E(N)$ of the spherical models, SJM-DFT, and nonspherical models, S'JM-DFT, UJM-DFT, and FP-DFT. From these figures, it is apparent that the improvement in the N dependence in $\Delta_2 E(N)$ from the nonspherical jellium models to the FP model that explicitly treats the ionic configuration is smaller as compared to that from the spherical models to the nonspherical models. Here it should be noted that the neutral charged UJM for Na_N shows surprisingly good agreement with an experiment for Na_{N+1}^+ in $\Delta_2 E(N)$ for $2 \leq N \leq 21$.[9,56]

As shown in Fig. 9(f), $\Delta_2 E_{\text{SJM-DFT}}(40)$ ($\Delta_2 E_{\text{S'JM-DFT}}(40)$) is positive. However, it is smaller than $\Delta_2 E_{\text{SJM-DFT}}(20)$, $\Delta_2 E_{\text{SJM-DFT}}(34)$, and $\Delta_2 E_{\text{SJM-DFT}}(58)$ [$\Delta_2 E_{\text{S'JM-DFT}}(20)$, $\Delta_2 E_{\text{S'JM-DFT}}(34)$, and $\Delta_2 E_{\text{S'JM-DFT}}(58)$]. On the other hand, as shown in Fig. 9(d), $\delta E_{\text{SJM-DFT}}(N)$ for $N=40$ is negative. Therefore, based on the definition of the magic number given in Eq. (10), $N=40$ is not a magic number in SJM-DFT. However, $N=40$ may be a magic number in S'JM-DFT and FP-DFT although $\delta E_{\text{FP-DFT}}(40)$ has a small positive value. Therefore, the magic feature at $N=40$ is expected to be weak in S'JM-DFT and FP-DFT. It is also expected that the consideration of the deviation from central force field in the total energy calculation is significant for obtaining a better agreement in N-dependent system stability with the experiment.

Here, it should be noted that $\Delta_2 E_{\text{SJM-DFT}}(68)$ is nearly 0 eV. As shown in Figs. 9(b) and 9(d), there is a large difference between $\Delta_2 E_{\text{expt}}(68) \sim 0$ eV and $\delta E_{\text{FP-DFT}}(68) \sim -0.5$ eV. From the similarity between the N dependence of $\delta E(N)$ and $\Delta_2 E(N)$, $\Delta_2 E_{\text{FP-DFT}}(68)$ is expected to differ significantly from $\Delta_2 E_{\text{expt}}(68)$ as compared to $\Delta_2 E_{\text{SJM-DFT}}(68)$. Therefore, it can be said that the N dependences of $\Delta_2 E_{\text{FP-DFT}}(N)$ and $\delta E_{\text{FP-DFT}}(N)$ are not necessarily more similar to that of $\Delta_2 E_{\text{expt}}(N)$ as compared to those of $\Delta_2 E_{\text{SJM-DFT}}(N)$ and $\delta E_{\text{SJM-DFT}}(N)$. However, insufficiency of

the stable geometry search for $N \geq 58$ can be related to these results, although this insufficiency does not affect to the main conclusion for the N dependent system stability for $N \leq 58$.

F. The possibilities for reducing the difference between the theoretically and experimentally obtained *N*-dependent system stability

We now consider the possibilities for reducing the difference between the theoretically and experimentally obtained N-dependent system stability. First, we discuss the possibility of improving in the magic number description based on the evaluation of the ground state energy. In the case of Na_N, it has already been shown that the N dependence of the experimental abundance peak at $N=5$, 6, and 7 cannot be expressed even in terms of $\Delta_2 E(N)$ of the configuration interaction calculations.[57,58] Therefore, it is expected that the improvement of the ground state energy evaluation will never lead to an improvement in the agreement for small values of N.

Thus for, several researchers have shown stable structures of Na_{40}.[40–42] In previous studies, a nearly spherical structure with high symmetry has not yet been obtained as the most stable structure. Instead of such a structure, we have found a structure with low symmetry (III) that is 0.320 eV more stable than structure (II), which is similar to the most stable structure found thus far.[40] The most stable structure, III, does not exhibit a strong peak for $N=40$ in $\delta E_{\text{FP-DFT}}(N)$. Further, energy differences between these structures are small. Therefore, we expect that $\delta E_{\text{FP-DFT}}(40)$ will not realize a strong magic feature even if a more stable structure is found in Na_{40}.

Within SJM, the N dependence of the energy per valence electron for Na_N was evaluated from a more precise FP calculation method called the diffusion Monte Carlo (DMC) calculation.[59] A weak magic feature was obtained for $N=40$ as a dip in the total energy versus N curve. From the result a weak magic feature is expected for $N=40$ in the N dependences of $\Delta_2 E_{\text{SJM-DMC}}(N)$ and $\delta E_{\text{SJM-DMC}}(N)$, in a manner similar to the cases of SJM-DFT and FP-DFT. However, by considering the explicit geometrical structure in DMC, the magic feature for $N=40$ can be strengthened as compared to that for $N=34$ and 58.

Second, we discuss the possibility of realizing improvements by a more proper evaluation of the system stability. In the experiments, the temperature in the apparatus is expected to be related to the final results. However, in the cluster study based on the total energy calculations, the temperature of the system is 0 K. If the consideration of the temperature is critical for the N-dependent system stability, instead of the internal energy $E(N)$, the free energy $F(N)$ must be considered. Further, the most stable and metastable structures of Na_N must be both considered properly for the N-dependent system stability. To consider the contribution of metastable structures, information about the potential energy surface or free energy landscape is required.

Finally, we discuss the possibility of realizing improvements from other viewpoints. In the case of Na_N, various shell models such as the Woods–Saxon type[3,12] and harmonic oscillator type[4] that neglect the Coulomb interactions between electrons exhibit a magic feature at $N=40$ in the N dependence of the shell correction energy and the curvature for the sum of the electronic eigenvalues. Further, it should be noted that the source of the larger HOMO-LUMO gap at $N=40$ compared to $N=34$ is attributed to the octupole deformation based on harmonic oscillator-type model,[60] and FP model.[41] These N dependences are strongly affected by the N dependence of the energy gap between the HOMO and the LUMO, i.e., the HOMO-LUMO gap. As shown in Fig. 10, within FP-DFT, the HOMO-LUMO gap for the most stable structure of Na_{40} is larger than that of Na_{34}. The absolute value of the HOMO-LUMO gap may be larger if the quasiparticle energy evaluated.[61] The improvement is significant if $I(N)$ in the abundance spectra of Na_N is a value that is more strongly related to the shell correction energy and the curvature of the sum of electronic eigenvalues as compared to $\Delta_2 E(N)$ or $\delta E(N)$.

As described in this section, by a more proper treatment of the system within the total energy calculations, discrepancies in the description of the N-dependent system stability with the experimental results can be reduced. However, this is difficult even in the case of the simplest metal cluster Na_N as shown here. For discussing the N-dependent cluster stability, various problems must first be solved. However, the magic number for the ground state, which avoids empirical parameter, is significant because it can be a standard to understand the N-dependent system stability. Further, for practical reasons, the evaluation method based on FP calculations is expected to retain the value in predictions of the experimental values of magic numbers.

V. ELECTRONIC STRUCTURES

A. Evolution of the electronic structure from atom to bulk

As described before, remarkable similarities are observed in the N dependence of the most and metastable structures and in the ground state energies of Na_N, Cu_N, and Ag_N clusters. These similarities are attributed to the N dependence of the electronic structure. In this section, N-dependent electronic structures for the most stable structures of each metal cluster are discussed.

Figure 10 shows the Kohn–Sham energy spectra for the most stable structures of the three metal clusters over the range of $1 \leq N \leq 75$ and ∞ (bulk). The density of states of the bulk crystal obtained from the band calculation is shown in the right-hand side space of each figure for the sake of comparison. Each Fermi level of the bulk crystal is set to the next HOMO-LUMO gap for the $N=75$ cluster. For all of the three figures, the space between HOMO and LUMO is colored blue. The red lines represent the occupied and unoccupied electronic energy levels.

For most values of N, the HOMO-LUMO gaps are small at odd values of N and large at even values of N, which results in the odd-even alternation of the HOMO-LUMO gaps. However, the HOMO-LUMO gap is large for several odd values of N and small for even values of N. Further, a

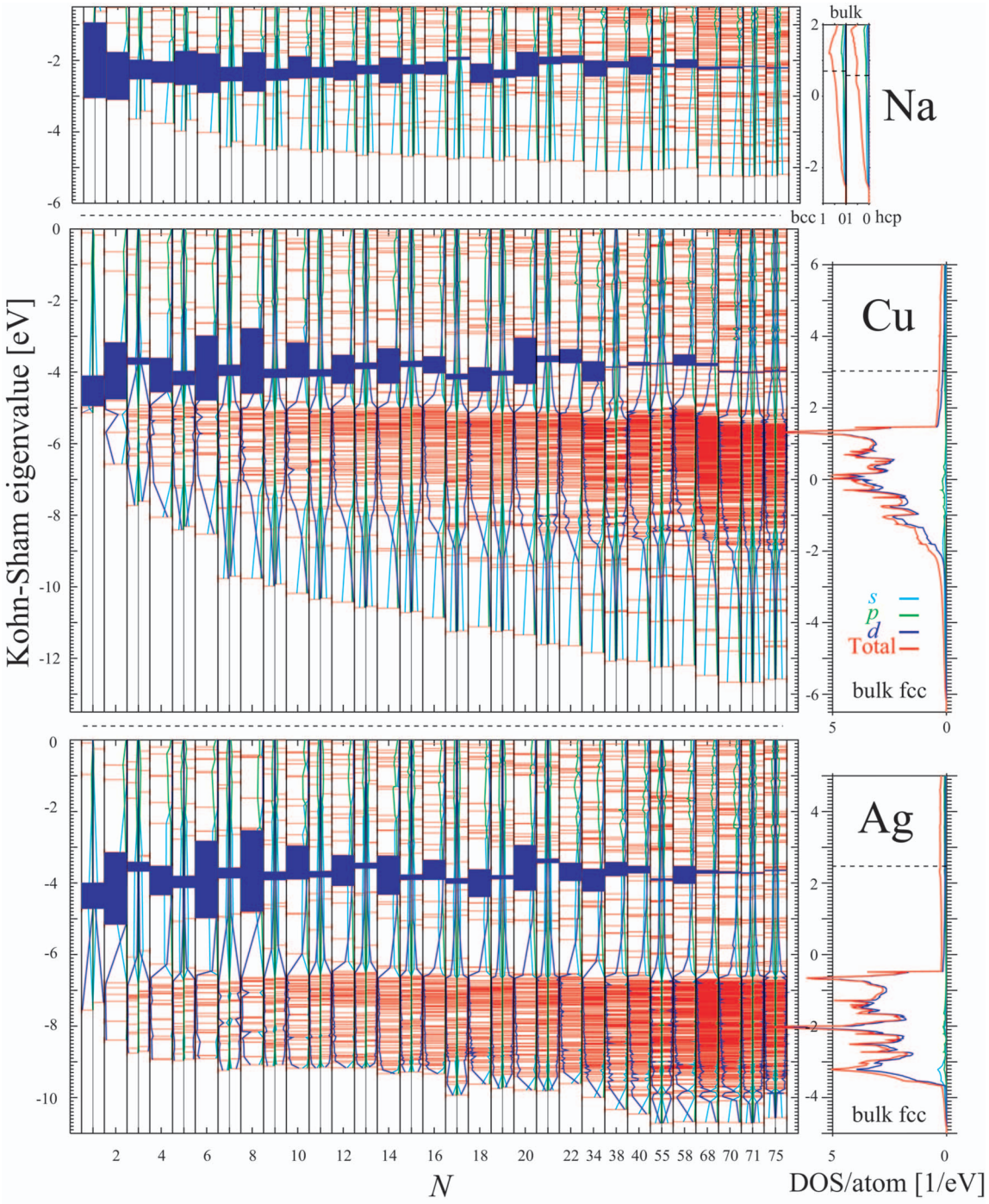

FIG. 10. *N* dependence of the Kohn–Sham eigenvalues from atom to bulk calculated for the most stable structures of Na_N, Cu_N, and Ag_N at $1 \leq N \leq 75$ and ∞ (bulk). The red lines indicate occupied and unoccupied electronic energy levels. For each spin-polarized system, the up spin states (left) and down spin states (right) are separated by a thin black line. The space between HOMO and LUMO is indicated in blue. Each projected value of *s*, *p*, and *d* to the Kohn–Sham state is connected by water, green, and blue lines, respectively. The density of states of each bulk crystal is shown to the right of each figure. Here, the Fermi level is represented by a dashed line. The Fermi level of a bulk crystal is arranged near the HOMO of the clusters composed of 75 atoms. Each colored line in the bulk crystal is the same as that in the case of clusters.

cluster that has a large HOMO-LUMO gap tends to have a lower HOMO and higher LUMO in the electronic structures. It should be noted that the odd-even alternation of the HOMO-LUMO gaps in Cu_N and Ag_N is significantly larger than that of Na_N for the benefit of *d* electrons. Further, the similarity in the odd-even alternation is more distinctive between the noble metal clusters. Generally, the HOMO-LUMO gap of each metal cluster converges to the Fermi level of the bulk crystal with increasing *N*.

For all of the metal clusters, with increasing *N*, the feature of each bulk energy band gradually appears in the electronic states. The energy width between the bottom and top of the occupied energy levels almost converges to that of the bulk crystal at $N=75$. In the case of Na_N, over a wide energy range, the states are characterized by *s* and *p*. In Cu_N and Ag_N, in addition to the *s*, and *p* characterized states similar to those shown in Na_N, energetically localized *d* band type states also appeared. It should be noted that the features of

localized d band in the bulk crystals already appeared at a rather small value of N in the width of the d states and the energetical distance from the top of the d states to the Fermi level. With increasing N, the strongly d characterized states gradually expand and almost converge to the width of the d band in each bulk crystal at $N=75$.

For the same type of geometrical structures as those described in Sec. IIA, distinctive similarities were also observed in the underwent splitting manner in which electronic states that are strongly characterized by s and p. As shown in Fig. 10, the energetical distances for the adjacent states strongly characterized by s and p are larger in Na_N than those of Cu_N and Ag_N. This relationship can be roughly understood from the relationship between the energetical distance for the adjacent states and the width of a well in the quantum well model, as described in the previous paper.[24] In this case, the s and p characterized electrons correspond to the quantum in the well. As shown in Figs. 4(a), 5, and 6(a)–6(d) for the existence of spatially and enegetically localized d electrons, closer interatomic distances are obtained in noble metal clusters as compared to those in alkali metal clusters. Namely, the width of the well is narrower in the noble metal clusters. As a result, larger energetical distances are realized in the noble metal clusters.

The stability of the spin-polarized state of the clusters is summarized as given below. For any odd N clusters, the stability of the spin-polarized state is higher than that of the spin-unpolarized state. On the other hand, for most even N clusters, the energy of the spin-unpolarized state is lower than that of the spin-polarized state. However, several structures that have high degeneracy in the neighborhood of the HOMO in the electronic state are exceptions. For a geometric structure with high symmetry, such as an icosahedron at $N=13$ and $N=55$, cuboctahedron at $N=38$, capped icosahedron at $N=71$, and Marks decahedron at $N=75$, the energy levels around HOMO are highly degenerated. Therefore, the high-spin states exhibit a higher stability than the low-spin states in systems such as an icosahedron for Na_{55} (Ref. 43) and Cu_{55}, although the case is opposite for Ag_{55}. However, for all of them, the energy differences between the high- and low-spin states are very small—0.033, 0.022, and 0.012 eV, respectively. The system is stabilized by lowering the symmetry from I_h to C_i in the structures based on the Jahn–Teller theorem.[45]

B. HOMO-LUMO gap, $E(N)$, and $v(N)/v(2)$ for the most and metastable clusters

In Sec. V A., only the electronic structure of the most stable cluster structure is discussed. In this section, the electronic structures of the most and metastable cluster structures are compared to understand the relationship between the geometric and electronic structures of the clusters. To save space, only the result of Na_N is presented. Figure 11 shows the HOMO-LUMO gap [(a) and (b)], $\Delta_2E(N)$ (a′), $\delta E(N)$ [(c) and (d)], and $v(N)/v(2)$ [(e) and (f)] of the most and metastable structures of Na_N clusters for $2\leq N\leq 22$ and $15\leq N\leq 75$, respectively. The values of the most stable structures are connected by a line. Several important features are observed from the comparison of the most and metastable structures, as described below.

A close correlation is observed between the HOMO-LUMO gap and $\Delta_2E(N)$ of the most stable structure. As shown in Figs. 11(a) and 11(a′), there is a strong correlation in the N dependence between them for a range of $2\leq N\leq 21$. Although the HOMO-LUMO gap considered in this study is the Kohn–Sham HOMO-LUMO gap, originally, the HOMO-LUMO gap is a physical value that corresponds to the difference between the ionization potential and the electron affinity in the system. The ionization potential of a neutral charged cluster composed of N atoms is defined as the energy difference between the total energy of the neutral cluster energy, $E(N,n)$, and the one electron detached charged cluster, $E(N,n-1)$. The electron affinity of a neutral charged cluster composed of N atoms is defined as the energy difference between the total energy of the neutral cluster, $E(N,n)$, and the one electron attached charged cluster, $E(N,n+1)$. Therefore, the HOMO-LUMO gap of a cluster composed of N atoms—HLG(N) is defined as $\mathrm{HLG}(N)\equiv E(N,n+1)+E(N,n-1)-2E(N,n)$. On the other hand, the energy curvature of a cluster composed of N atoms, $\Delta_2E(N)$, is defined as $\Delta_2E(N)\equiv E(N+1,n)+E(N-1,n)-2E(N,n)$. Although they are clearly different physical values, the forms of these two types of values are very similar. The relation described above should be studied in detail in the future.

Generally, as shown in Figs. 11(a) and 11(b), the most stable structures exhibit a relatively large HOMO-LUMO gap. Further, as shown in Fig. 10, a cluster that has a large HOMO-LUMO gap tends to have a lower HOMO and higher LUMO in the electronic structures, as described in Sec. V A. However, from a comparison with the energy differences between the most and metastable structures from $\delta E(N)$ shown in Figs. 11(c) and 11(d), it is apparent that a large HOMO-LUMO gap is not a necessary condition for the most stable structure. For example, in Na_4, the metastable structure III exhibits a larger HOMO-LUMO gap than that of the most stable structure I. Although it is not shown in this paper, the same type of example can also be shown for Cu_N and Ag_N.

Finally, the N dependence of the normalized cluster volume $v(N)/v(2)$ of the most and metastable structures, and the relation to the total energy and the HOMO-LUMO gap is noted. As shown in Figs. 11(e) and 11(f), it is apparent that the cluster volume is directly dependent on the structural type, namely, L, P, O, and C. From the system stability, as shown in Figs. 11(c) and 11(d), it is apparent that the most stable structures do not necessarily have a minimum value of $v(N)/v(2)$. Further, the N dependence of $v(N)/v(2)$ for $N\geq 7$ does not change significantly if energetically closed structural isomers to the most stable structures are also considered. As shown in the figure, it is apparent that the relationship between the HOMO-LUMO gap and $v(N)/v(2)$ for the most and metastable structures cannot be simplified.

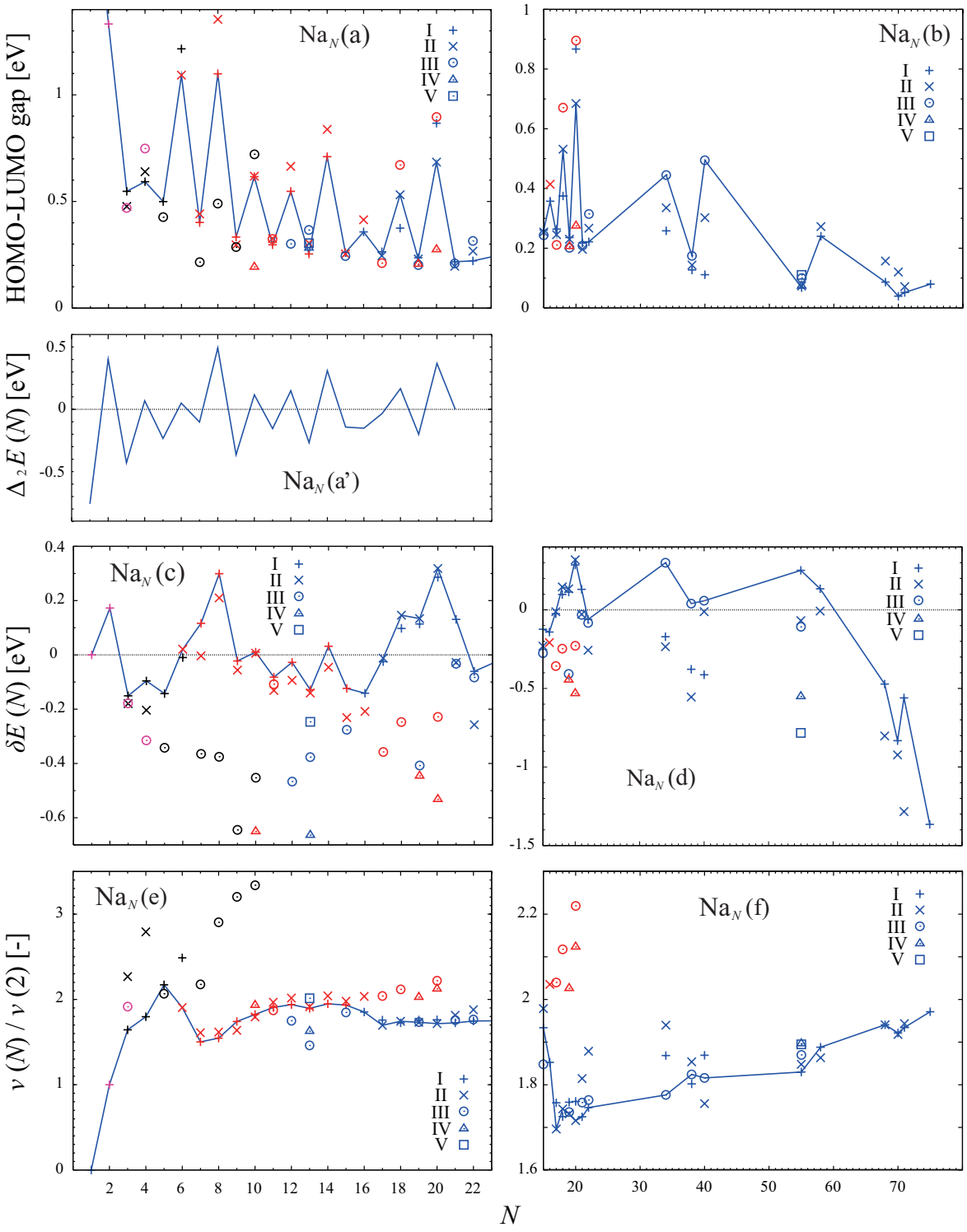

FIG. 11. (a) and (b) show the N dependence of the HOMO-LUMO energy gaps of Na_N for the most and metastable structures at $1 \leq N \leq 22$ and $15 \leq N \leq 75$, respectively. (a′) shows the N dependence of $\Delta_2 E(N)$ for the most stable structures of Na_N at $1 \leq N \leq 21$. (c) and (d) show the N dependence of $\delta E(N)$ for Na_N for the most and metastable structures at $1 \leq N \leq 22$ and $15 \leq N \leq 75$, respectively. (e) and (f) show the N dependence of $v(N)/v(2)$ for Na_N for the most and metastable structures at $1 \leq N \leq 22$ and $15 \leq N \leq 75$, respectively. Each type of structure, namely, linear (L), planar (P), opened (O), and closed (C), is indicated by purple, black, red, and blue, respectively. For each figure, the values of the most stable structures are connected by a line.

VI. CONCLUSIONS

The N-dependent geometric structure, system stability, and electronic structures of Na_N, Cu_N, and Ag_N metal clusters are studied in detail for a range of $2 \leq N \leq 75$ based on the DFT. Strong similarities are observed between the three different metal clusters. These similarities that originate from the outermost is s electron in the alkali and noble metal atoms composing each cluster. Much stronger similarities are observed between the two noble metal clusters for the benefit of d electrons. The most stable structures are the same for the three different metal clusters for approximately half the clus-

TABLE I. The averaged nearest neighbor diatomic distance d, binding energy per atom E_b/N, and bulk modulus B_0 of dimers and bulk crystals for Na, Cu, and Ag in the equilibrium position evaluated from the DFT (Refs. 1 and 2)-GGA [PW91 (Ref. 28)] calculations in this study and other studies based on several experiments are presented.

		d (Å)		E_b/N (eV/atom)		B_0 (10^{11} N/m^2)
Element	Type of data	Dimer	Bulk	Dimer	Bulk	Bulk
Na	This study	3.07	3.64	0.38	1.07	0.074
	Expt.	3.079[a]	3.659[b]	0.379[a]	1.113[b]	0.068[b]
Cu	This study	2.22	2.57	1.14	3.53	1.396
	Expt.	2.220[a]	2.55[b]	0.915[a]	3.49[b]	1.37[b]
Ag	This study	2.58	2.95	0.89	2.53	0.876
	Expt.	2.531[c]	2.89[b]	0.831[a]	2.95[b]	1.007[b]

[a]Reference 46.
[b]Reference 47.
[c]Reference 48.

ter sizes N considered in this study. Even if the most stable structures are different, the same type of structures is obtained if the metastable structures are also considered. For all of the three clusters, the structural type of the most stable structure changes in the order $L \rightarrow P \rightarrow O \rightarrow C$ with increasing N. This structural-type transition leads to a deviation from the monotonic increase in specific volume with N. A remarkable similarity is also observed for the N dependence of cluster energy $E(N)$ for the most stable geometric structures. This similarity is related to the similarity in the electronic structures. The amplitude of this energy difference is larger in the two noble metal clusters than in the alkali metal cluster. This is attributed to the contribution of the d electrons to the bonds. The magic number is explicitly defined with a new criterion in the framework of total energy calculations. In the case of Na_N, a semiquantitative comparison between the experimental abundance spectra[3] and the total energy calculations is carried out. For the improvement of the agreement with the experimental result, several possibilities arise for the total energy calculations. The changing aspects of the Kohn–Sham eigenvalues from $N=2$ to $N=75$ are presented for the three different metal clusters. The features of the bulk density of states already appeared at $N=75$ for all of the three clusters. With increasing values of N, the HOMO-LUMO gap clearly exhibits an odd-even alternation and converges to 0. This alternation is a specific feature of alkali and noble metal clusters in which each element has one s electron in the outermost shell. It is also found that in some cases, the HOMO-LUMO gap is large at odd value of N and small at even value of N. Although there is similarity in the N dependence of the HOMO-LUMO gap between the three metal clusters, it is much stronger between the two noble metal clusters. The spatially localized d electrons in the noble metals are energetically localized. The growth aspect of the d band below the Fermi level of the noble metal clusters with increasing N is presented. A good correspondence is obtained in the d characteristic of the electronic states between the cluster composed of 75 atoms and the bulk metal.

ACKNOWLEDGMENTS

The authors gratefully acknowledge the kind hospitality at the Institute for Materials Research and the staff of the Center for Computational Materials Science for allowing the use of the Hitachi SR8000/64 supercomputing facilities. The authors are grateful to Professor Bernd von Issendorff for sharing his results prior to publication and Dr. Koichi Yoshizaki for allowing us to refer to his thesis prior to publication. M.I. deeply acknowledges valuable knowledge and supports in molecular dynamics simulation for clusters from Dr. Tamio Ikeshoji, valuable knowledge about group theory from Dr. Kenta Hongo, and valuable discussions and various supports from Professor Hiroshi Yasuhara. M.I. deeply acknowledges Dr. Soh Ishii for developing foundation of the study.

APPENDIX A: COMPARISON IN THE BASIC PROPERTIES EVALUATED FROM THE FIRST PRINCIPLES CALCULATIONS AND EXPERIMENTS

See Table I.

APPENDIX B: RELATION BETWEEN THE SPECIFIC VOLUMES AND MELTING POINTS

Figure 12(a) shows $v(N)/v(2)$ of the most stable structure (icosahedron) of Na_N for $N=55$, 147, and 309 obtained in our previous study.[43] Here, $v(N)/v(2)$ increases monotonically with N. Figure 12(b) shows the melting points T_m of the Na_N cluster at $N=55$, 147, and 309, as observed by Haberland *et al.*,[62] to discuss the relationship with cluster volumes. T_m decreases monotonically with increasing N. This N dependence of T_m is in contrast to the trend observed in the case of the cluster volume. Aguado and Löpez[63] showed that the volume $v(N)$ and T_m of the most stable structures of the Na_N cluster exhibited an opposite trend for $N \geq 55$ from the molecular dynamics calculations based on DFT-LDA. This conclusion supports the existence of a relationship between the N dependence of $v(N)/v(2)$ as evaluated by us and that of the T_m observed by Habarland *et al.* Further, the more precise DFT-LDA molecular dynamics calculations predict that T_m of Na_{40} is higher than that of Na_{55}.[40] T_m of Na_{40} has

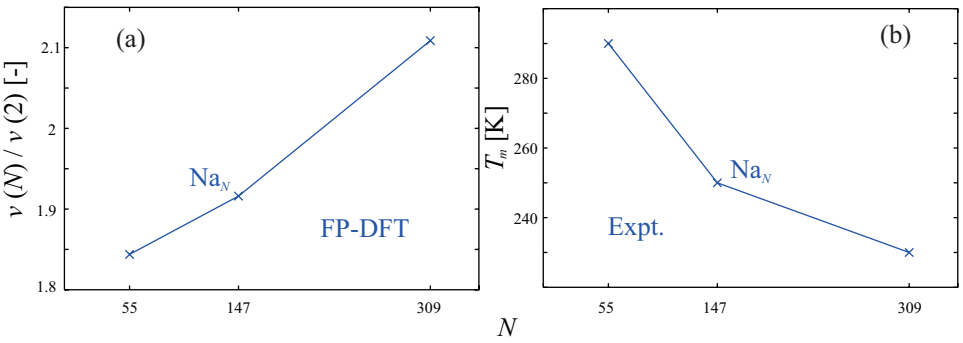

FIG. 12. (a) shows the N dependence of $v(N)/v(2)$ for Na_N (N=55, 147, and 309), while (b) shows the N dependence of the melting point T_m observed by Haberland *et al.* (Ref. 62).

not yet been observed experimentally. Our calculation results of $v(N)/v(2)$ shown in Figs. 6(a) and 6(b) do not contradict with the result of the DFT-LDA molecular dynamics study[40] with regard to the relationship between Na_{40}, and Na_{55}.

If the conclusion about the relation between the cluster $v(N)$ or $v(N)/v(2)$ and T_m in Na_N holds for Cu_N and Ag_N for $N \leq 55$, it is expected that T_m of Cu_{40} and Ag_{40} are lower than that of Cu_{55} and Ag_{55}, respectively. For $N \leq 22$, the volume of the most stable cluster changes significantly with the structural-type transitions ($L \rightarrow P \rightarrow O \rightarrow C$) described in Sec. III A. Therefore, for $N \leq 22$, the N dependence of the cluster T_m is expected to reflect this change.

[1] P. Hohenberg and W. Kohn, Phys. Rev. **136**, B864 (1964).
[2] W. Kohn and L. J. Sham, Phys. Rev. **140**, A1133 (1965).
[3] W. D. Knight, K. Clemenger, W. A. de Heer, W. A. Saunders, M. Y. Chou, and M. L. Cohen, Phys. Rev. Lett. **52**, 2141 (1984).
[4] K. Clemenger, Phys. Rev. B **32**, 1359 (1985).
[5] J. L. Martins, R. Car, and J. Buttet, Surf. Sci. **106**, 265 (1981).
[6] M. Y. Chou, A. Cleland, and M. L. Cohen, Solid State Commun. **52**, 45 (1984).
[7] W. Ekardt, Phys. Rev. B **29**, 1558 (1984).
[8] M. Koskinen, P. O. Lipas, and M. Manninen, Z. Phys. D: At., Mol. Clusters **35**, 285 (1995).
[9] H. Häkkinen, J. Kolehmainen, M. Koskinen, P. O. Lipas, and M. Manninen, Phys. Rev. Lett. **78**, 1034 (1997).
[10] M. Moseler, B. Huber, H. Häkkinen, U. Landman, G. Wrigge, M. A. Hoffmann, and B. v. Issendorff, Phys. Rev. B. **68**, 165413 (2003).
[11] C. A. Utreras-Díaz and H. B. Shore, Phys. Rev. B **40**, 10345 (1989).
[12] H. Nishioka, K. Hansen, and B. R. Mottelson, Phys. Rev. B **42**, 9377 (1990).
[13] S. Bjørnholm, J. Borggreen, O. Echt, K. Hansen, J. Pedersen, and H. D. Rasmussen, Phys. Rev. Lett. **65**, 1627 (1990).
[14] O. Genzken and M. Brack, Phys. Rev. Lett. **67**, 3286 (1991).
[15] S. M. Reimann, M. Brack, and K. Hansen, Z. Phys. D: At., Mol. Clusters **28**, 235 (1993).
[16] C. Yannouleas and U. Landman, Phys. Rev. B **48**, 8376 (1993).
[17] W. A. de Heer, Rev. Mod. Phys. **65**, 611 (1993).
[18] M. Brack, Rev. Mod. Phys. **65**, 677 (1993).
[19] V. Kumar, K. Esfarjani, and Y. Kawazoe, in *Clusters and Nanomaterials*, edited by Y. Kawazoe, T. Kondow, and K. Ohno (Springer, New York, 2001), p. 9.
[20] W. A. de Heer, W. D. Knight, M. Y. Chou, and M. L. Cohen, Solid State Phys. **40**, 93 (1987).
[21] J. L. Martins, J. Buttet, and R. Car, Phys. Rev. Lett. **53**, 655 (1984).
[22] U. Röthlisberger and W. Andreoni, J. Chem. Phys. **94**, 8129 (1991).
[23] L. Kronik, I. Vasiliev, M. Jain, and J. R. Chelikowsky, J. Chem. Phys. **115**, 4322 (2001).
[24] M. Itoh, V. Kumar, and Y. Kawazoe, Int. J. Mod. Phys. B **19**, 2421 (2005).
[25] References in Ref. 24.
[26] M. Yang, K. A. Jackson, C. Koehler, T. Frauenheim, and J. Jellinek, J. Chem. Phys. **124**, 024308 (2006).
[27] M. Yang, K. A. Jackson, and J. Jellinek, J. Chem. Phys. **125**, 144308 (2006).
[28] J. P. Perdew, J. A. Chevary, S. H. Vosko, K. A. Jackson, M. R. Pederson, D. J. Singh, and C. Fiolhais, Phys. Rev. B **46**, 6671 (1992).
[29] D. Vanderbilt, Phys. Rev. B **41**, 7892 (1990).
[30] P. Pulay, Chem. Phys. Lett. **73**, 393 (1980).
[31] D. M. Wood and A. Zunger, J. Phys. A **18**, 1343 (1985).
[32] M. C. Payne, M. P. Teter, D. C. Allan, T. A. Arias, and J. D. Joannopoulos, Rev. Mod. Phys. **64**, 1045 (1992).
[33] Cambridge cluster database, http://www-wales.ch.cam.ac.uk/CCD.html.
[34] G. Wrigge, M. A. Hoffmann, and B. v. Issendorff, Phys. Rev. A. **65**, 063201 (2002).
[35] H. Häkkinen, M. Moseler, O. Kostko, N. Morgner, M. A. Hoffmann, and B. v. Issendorff, Phys. Rev. Lett. **93**, 093401 (2004).
[36] O. Kostko, N. Morgner, M. A. Hoffmann, and B. v. Issendorff, Eur. Phys. J. D. **34**, 133 (2005).
[37] O. Kostko, B. Huber, M. Moseler, and B. v. Issendorff, Phys. Rev. Lett. **98**, 043401 (2007).
[38] H. J. Monkhorst and J. D. Pack, Phys. Rev. B **13**, 5188 (1976).
[39] G. Kresse and J. Furthmüller, Phys. Rev. B **54**, 11169 (1996).
[40] M.-S. Lee, S. Chacko, and D. G. Kanhere, J. Chem. Phys. **123**, 164310 (2005).
[41] A. Rytkönen, H. Häkkinen, and M. Manninen, Phys. Rev. Lett. **80**, 3940 (1998).
[42] S. M. Ghazi, M.-S. Lee, and D. G. Kanhere, J. Chem. Phys. **128**, 104701 (2008).
[43] M. Itoh, V. Kumar, and Y. Kawazoe, Phys. Rev. B **73**, 035425 (2006).
[44] V. Kumar and R. Car, Z. Phys. D: At., Mol. Clusters **19**, 177 (1991).
[45] H. A. Jahn and E. Teller, Proc. R. Soc. London, Ser. A **161**, 220 (1937).
[46] *Handbook of Chemistry and Physics*, 85th ed., edited by D. R. Lide (CRC, Boca Raton, 2004).
[47] C. Kittel, *Introduction to Solid State Physics* (Wiley, New York, 1996).
[48] B. Simard, P. A. Hackett, A. M. James, and P. R. R. Langridge-Smith, Chem. Phys. Lett. **186**, 415 (1991).
[49] N. Takeuchi, C. T. Chan, and K. M. Ho, Phys. Rev. B **40**, 1565 (1989); P. H. T. Philipsen and E. J. Baerends, *ibid.* **61**, 1773 (2000); T. Nautiyal, S. J. Youn, and K. S. Kim, *ibid.* **68**, 033407 (2003); B. Zhou and E. A. Carter, J. Chem. Phys. **122**, 184108 (2005).
[50] M. Manninen, J. Mansikka-aho, H. Nishioka, and Y. Takahashi, Z. Phys. D: At., Mol. Clusters **31**, 259 (1994).
[51] I. Katakuse, T. Ichihara, Y. Fujita, T. Matsuo, T. Sakurai, and H. Matsuda, Int. J. Mass Spectrom. Ion Process. **67**, 229 (1985).
[52] I. Katakuse, T. Ichihara, Y. Fujita, T. Matsuo, T. Sakurai, and H. Matsuda, Int. J. Mass Spectrom. Ion Process. **74**, 33 (1986).
[53] R. Rabinovitch, C. Xia, and V. V. Kresin, Phys. Rev. A **77**, 063202 (2008).
[54] From Fig. 2 in Ref. 3, we confirmed that $\Delta_2 E_{\text{expt}}(N)$ is not changed significantly by changing the Ar gas pressure in the first step in the experiment.
[55] W. Ekardt and Z. Penzar, Phys. Rev. B **38**, 4273 (1988).
[56] C. Bréchignac, Ph. Cahuzac, J. Leygnier, and J. Weiner, J. Chem. Phys. **90**, 1492 (1989).
[57] V. Bonačić-Koutecký, P. Fantucci, and J. Koutecký, Phys. Rev. B **37**, 4369 (1988).
[58] V. Bonačić-Koutecký, I. Boustani, M. Guest, and J. Koutecký, J. Chem. Phys. **89**, 4861 (1988).
[59] J. Tao, J. P. Perdew, L. M. Almeida, C. Fiolhais, and S. Kümmel, Phys. Rev. B **77**, 245107 (2008).
[60] I. Hamamoto, B. Mottelson, H. Xie, and X. Z. Zhang, Z. Phys. D: At., Mol. Clusters **21**, 163 (1991).
[61] K. Yoshizaki, M.S. thesis, Tohoku University, 1996. In this thesis, based

on various approximations to the exchange-correlation energy functional within SJM-DFT under LDA, time dependent LDA (TDLDA), and random phase approximation (RPA), the HOMO-LUMO gaps of Na_N clusters are evaluated in a range of $N \leq 40$. For $N=34$ and 40, the HOMO-LUMO gaps are evaluated as 0.45 (LDA), 1.45 (TDLDA), 1.50 (RPA), and 0.20 (LDA), 1.10 (TDLDA), 1.30 (RPA), respectively. If the ionic configurations are considered, the values are expected to be changed.

[62] H. Haberland, T. Hippler, J. Donges, O. Kostko, M. Schmidt, and B. v. Issendorff, Phys. Rev. Lett. **94**, 035701 (2005).
[63] A. Aguado and J. M. Löpez, Phys. Rev. Lett. **94**, 233401 (2005).